

Safe-Subspace Pseudo-Label Refinement for Source-Free Graph Domain Adaptation

Yingxu Wang, Xinwang Liu, Siyang Gao, Nan Yin

Abstract—Source-free graph domain adaptation (SF-GDA) aims to adapt source-trained graph models to unlabeled target graphs when source graphs are no longer accessible. A central obstacle is pseudo-label reliability: under feature and topological shifts, source-induced predictions may become confidently wrong, and indiscriminate self-training can amplify systematic errors through graph message passing. This paper studies SF-GDA from a selective pseudo-labeling perspective. Instead of assuming globally bounded pseudo-label noise over the entire target domain, we identify a confidence-consistent safe subspace on which pseudo-label noise can be controlled under restricted posterior discrepancy, and derive a target-risk decomposition that separates safe-subspace fitting error, selected-label noise, and uncertain-set risk. Guided by this analysis, we propose Safe-Subspace Pseudo-Label Refinement (S^2 PLR), a source-free graph adaptation framework that applies hard pseudo-label supervision only to target graphs supported by both semantic and structural evidence. Specifically, S^2 PLR estimates semantic reliability using source-committee confidence and disagreement, learns a target-intrinsic structural representation via graph contrastive learning, verifies pseudo-labels through neighborhood consistency, and exploits the remaining uncertain samples with noise-tolerant soft regularization rather than unreliable hard labels. Experiments on image and real-world graph benchmarks under different domain shifts demonstrate that S^2 PLR achieves robust and competitive performance across diverse source-free transfer settings.

Index Terms—Graph Neural Networks, Source-Free Domain Adaptation, Noisy Label Learning

I. INTRODUCTION

Graph data are ubiquitous in social networks, biological systems, and molecular discovery, yet models trained on one graph domain often suffer substantial performance degradation when deployed on another because distribution shifts may arise in both node attributes and topology [1–6]. Graph domain adaptation (GDA) addresses this challenge by transferring knowledge from labeled source graphs to unlabeled target graphs and has become an important paradigm for robust graph representation learning [7–10]. However, most existing GDA methods assume that source graphs remain accessible during adaptation, which is often unrealistic because of privacy, proprietary, and storage constraints. This limitation motivates source-free domain adaptation, where adaptation is performed using only a pretrained source model and unlabeled target

data [11–13]. Extending this setting to graph-structured data gives rise to source-free graph domain adaptation (SF-GDA), a substantially more challenging problem because domain shift affects not only feature distributions but also relational structures and message-passing behavior [14–18].

A central difficulty in SF-GDA is that target adaptation must rely on pseudo supervision induced by a fixed source hypothesis. Such pseudo-labels can be systematically biased under target-side structural shift, and recent source-free adaptation analyses show that full-domain self-training may enter an unbounded-noise regime in which a source classifier is confidently wrong on part of the target domain [19–21]. This failure mode is especially consequential for graph data: an erroneous pseudo-label is not an isolated classification mistake, but can be propagated through neighborhood aggregation and may distort both local structural consistency and global representation geometry. Thus, the key question in SF-GDA is not merely how to refine pseudo-labels, but which target samples can be trusted for hard supervision and which should be handled only through softer target-side regularization.

Existing SF-GDA methods have made important empirical progress through topology-aware alignment, collaborative pseudo-label refinement, and structure-preserving self-supervision [15–17, 22]. Nevertheless, most of them do not explicitly characterize the reliability region on which pseudo-label training is theoretically justified. Confidence filtering alone is insufficient because a source model may make overconfident target errors, whereas neighborhood consistency alone can be misleading if the target representation is geometrically distorted. Moreover, discarding all uncertain samples wastes target distributional information, while assigning hard pseudo-labels to them risks negative transfer. These observations call for a selective adaptation framework that (i) identifies a reliable target subspace using both semantic confidence and structural evidence, (ii) learns a compact target-intrinsic geometry for neighborhood verification, and (iii) regularizes the remaining uncertain samples without treating their pseudo-labels as ground truth.

In this work, we develop such a framework by revisiting pseudo-label noise in source-free graph domain adaptation from a selective-risk perspective. Rather than claiming that pseudo-label noise is globally bounded over the entire target domain, we establish sufficient conditions under which it is bounded on a confidence-consistent safe subspace. Our analysis explicitly separates two aspects that are often conflated: source confidence and posterior discrepancy determine the population-level pseudo-label noise bound, while neighborhood consistency and geometric compactness provide target-

Yingxu Wang is with Department of Computer Science and Engineering, Chinese University of Hong Kong. E-mail: yingxu.wang@gmail.com.

Xinwang Liu is with College of Computer, National University of Defense Technology, Changsha, 410073, China. E-mail: xinwangliu@nudt.edu.cn.

Siyang Gao is with Department of Data Science, City University of Hong Kong. E-mail: siyangao@city.edu.hk.

Nan Yin is with The Education University of Hong Kong, Hong Kong. E-mail: yinnan8911@gmail.com.

only evidence for identifying reliable samples in practice. This distinction avoids overclaiming beyond the assumptions and leads to an actionable risk decomposition: hard pseudo-label supervision should be restricted to the safe subspace, and the residual uncertain set should be controlled by soft regularization. Motivated by this selective-risk analysis, we propose Safe-Subspace Pseudo-Label Refinement (S²PLR), a selective-risk-guided framework for source-free graph domain adaptation. S²PLR first estimates reliable target supervision through multi-expert uncertainty quantification, then learns a target-intrinsic structural manifold via self-supervised graph contrastive learning, and subsequently performs dual-view nested pseudo-label refinement to identify safe target samples. For the remaining uncertain samples, S²PLR applies noise-tolerated regularization so that their distributional information can still be exploited without propagating incorrect hard pseudo-labels. In this way, S²PLR connects selective bounded-noise analysis with structure-aware graph adaptation, moving beyond purely empirical pseudo-label refinement or topology alignment [15–17]. The main contributions of this work are summarized as follows:

- We provide a selective theoretical analysis of pseudo-label noise in SF-GDA. Under an explicit restricted posterior-discrepancy assumption, the analysis derives a pseudo-label noise bound on a confidence-qualified target subset and decomposes the resulting target risk into safe-subspace fitting error, selected-label noise, and uncertain-set risk.
- We propose S²PLR, a source-free graph domain adaptation framework that integrates multi-expert uncertainty quantification, target-intrinsic structure learning, dual-view nested pseudo-label refinement, and noise-tolerated regularization according to the reliability and risk factors identified by the analysis.
- We evaluate S²PLR on image and graph benchmarks under different domain shifts. The results show that S²PLR achieves competitive performance in most transfer settings.

II. RELATED WORK

a) Source-Free Domain Adaptation and Graph Domain Adaptation: Source-free domain adaptation (SFDA) transfers a source-trained model to an unlabeled target domain when source samples are no longer accessible during adaptation [23–27]. Existing SFDA methods commonly rely on information maximization, self-training, pseudo-label refinement, feature consistency, or confidence calibration to adapt the source decision boundary to the target distribution [19, 27–30]. Source-free graph domain adaptation (SF-GDA) extends this setting to graph-structured data, where domain shifts may affect both node attributes and graph topology [11, 15, 17, 31–33]. This makes adaptation more challenging than in Euclidean data because message passing can amplify local structural mismatch and propagate pseudo-label errors across graph neighborhoods. Recent SF-GDA methods address these issues through topology reconstruction, contrastive learning, graph collaborative training, and structure-aware representation alignment [7, 34–36]. Different from topology-alignment methods that primarily reduce representation mismatch, S²PLR focuses on

the reliability of the pseudo-supervision used during source-free adaptation. It explicitly separates target samples into a safe subspace for hard pseudo-label supervision and an uncertain set for soft regularization. This selective formulation differs from conventional confidence filtering because target-side structural consistency is used as an additional label-free certificate before a pseudo-label is allowed to affect supervised adaptation.

b) Learning with Noisy Labels and Pseudo-Label Reliability: Learning with noisy labels has been widely studied in supervised learning, where common strategies include robust losses, sample selection, label correction, co-training, and uncertainty-aware reweighting [37–41]. In SFDA, pseudo-label noise differs from ordinary annotation noise because it is induced by applying a fixed source hypothesis to a shifted target distribution. Such noise can be systematic rather than random, and recent analyses show that full-domain source-free self-training may suffer from unbounded pseudo-label noise under severe domain shift [19, 20]. For graph data, the issue is further complicated by structural heterogeneity: overconfident pseudo-labels may be locally unsupported, while neighborhood agreement may be unreliable if the target representation is geometrically distorted. S²PLR therefore combines multi-expert uncertainty estimation, target-intrinsic structural learning, and nested pseudo-label refinement to identify a confidence-consistent safe subspace. This design is complementary to existing noisy-label learning methods because it treats pseudo-label reliability as a selective adaptation problem under source-free graph shifts rather than as a standard label-corruption problem.

III. REVISITING THEORETICAL ANALYSIS OF LABEL NOISE IN SF-GDA

A. Source-Free Graph Domain Adaptation

We consider source-free graph domain adaptation (SF-GDA) for graph-level classification [11, 15–17]. Let a graph be denoted by $G = (V, E, \mathbf{X})$, where V and $E \subseteq V \times V$ are the node and edge sets, respectively, and $\mathbf{X} \in \mathbb{R}^{|V| \times d}$ is the node-feature matrix. During source pretraining, a classifier h_S is learned from a labeled source domain $\mathcal{D}_S = \{(G_i^S, y_i^S)\}_{i=1}^{n_S} \sim P_S(G, Y)$. During adaptation, source graphs are unavailable, and the learner only has access to the pretrained source model h_S and an unlabeled target domain $\mathcal{D}_T = \{G_j^T\}_{j=1}^{n_T} \sim P_T(G)$, where the two domains share the same label space $\mathcal{Y} = \{1, \dots, C\}$ but follow different graph distributions due to shifts in both node attributes and topology [7, 8]. The objective of SF-GDA is to learn a target model h_T that adapts h_S to \mathcal{D}_T without revisiting source data and minimizes the target risk $R_T(h_T) = \Pr_{(G, Y) \sim P_T} [h_T(G) \neq Y]$.

B. Setup and Theoretical Question

We analyze source-free graph domain adaptation in the induced target representation space, as commonly adopted in prior SF-GDA methods [15–17]. Specifically, each target graph $G \in \mathcal{D}_T$ is mapped to a representation $x = \phi(G) \in \mathcal{X}$, and we denote the set of target representations by $\mathcal{X}_T = \{\phi(G) \mid G \in \mathcal{D}_T\}$. In the source-free setting, a source model

h_S is trained on the labeled source domain and then deployed on unlabeled target samples only. The learner has no access to source graphs during adaptation and must rely on pseudo-labels induced by the source model,

$$\tilde{y}(x) = \arg \max_{y \in \mathcal{Y}} p_S(y | x),$$

where $p_S(y | x)$ denotes the posterior predicted by the source model. Therefore, the success of source-free adaptation fundamentally depends on whether these source-induced pseudo-labels remain reliable under domain shift [11, 19, 20].

To formalize this issue, we define the instance-wise pseudo-label noise rate on the target domain as

$$\eta(x) = \Pr_{Y \sim p_T(\cdot | x)} [\tilde{y}(x) \neq Y] = 1 - p_T(\tilde{y}(x) | x),$$

where $p_T(y | x)$ denotes the target posterior. In conventional learning with label noise, effective training typically relies on the bounded-noise premise that the corrupted label remains positively correlated with the ground truth. In source-free adaptation, however, the pseudo-label $\tilde{y}(x)$ is produced by a fixed source classifier on a shifted target distribution, so the resulting noise is a structured consequence of domain mismatch rather than random corruption [19, 20]. For graph data, this issue is further entangled with target geometry and local structural relations, since neighborhood consistency may either support or contradict a pseudo-label in the learned representation space.

These observations lead to the central theoretical question of this work: *Can pseudo-label noise in SF-GDA be bounded under domain and structural shifts, and if so, on which subset of target samples can such a guarantee be established?* Equivalently, rather than assuming that there exists a constant $\bar{\eta} < 1/2$ such that

$$\eta(x) \leq \bar{\eta}, \quad \forall x \in \mathcal{X}_T,$$

we ask whether one can identify a restricted subset $\mathcal{H} \subseteq \mathcal{X}_T$ on which the bounded-noise condition is restored, while the remaining samples are handled more cautiously. Answering this question is essential for justifying pseudo-label-based adaptation in SF-GDA. In the following, we first revisit the existing unbounded-noise theory in source-free adaptation, then analyze its scope, and finally establish a bounded-noise result within a confidence-consistent safe subspace.

C. Existing Unbounded-Noise Theory

To answer the question raised above, we revisit recent theoretical analyses of label noise in source-free adaptation through the lens of learning with label noise [19, 20]. In conventional learning with noisy labels, a standard premise is that the noisy supervision remains bounded, namely, there exists a constant $\bar{\eta} < 1/2$ such that

$$\eta(x) \leq \bar{\eta}, \quad \forall x \in \mathcal{X}_T.$$

This condition ensures that the observed label is still positively correlated with the ground-truth label, which underlies the validity of robust loss correction and noise-tolerant optimization. In source-free adaptation, however, the pseudo-label $\tilde{y}(x)$ is

not generated by random corruption. Instead, it is induced by applying a fixed source classifier to a shifted target distribution, making the resulting noise structurally determined by domain mismatch rather than stochastic perturbation [19, 20].

Following [20], consider a binary classification setting in which the source domain is modeled as a Gaussian mixture:

$$x | y = k \sim \mathcal{N}(\mu_k, \sigma^2 I_d), \quad k \in \{1, 2\},$$

while the target domain is a globally shifted version of the source:

$$x | y = k \sim \mathcal{N}(\mu_k + \Delta, \sigma^2 I_d), \quad k \in \{1, 2\},$$

where $\Delta \in \mathbb{R}^d$ denotes the class-invariant translation vector. A key quantity governing the noise behavior is the projection of the domain shift onto the class-separation direction,

$$\alpha = \frac{\Delta^\top (\mu_2 - \mu_1)}{\|\mu_2 - \mu_1\|^2}.$$

Under this setup, the pseudo-label noise is shown to be unbounded in a precise conditional sense.

Theorem 1 (Unbounded Label Noise in SFDA [20]). Suppose $\alpha \neq 0$. Then there exists a non-empty region $\mathcal{R} \subseteq \mathcal{X}_T$, referred to as a mislabeling area, such that for any $\delta \in (0, 1)$, if

$$\alpha > \frac{1}{d} \log \frac{1 - \delta}{\delta},$$

the conditional error of the source classifier on \mathcal{R} satisfies

$$\Pr_{(x,y) \sim P_T} [h_S(x) \neq y | x \in \mathcal{R}] \geq 1 - \delta.$$

Theorem 1 shows that, under domain shift, the source classifier can be not merely uncertain but systematically and even confidently wrong on a non-empty target region. In other words, the pseudo-label error rate may exceed the usual learnable regime and can approach one within the mislabeling area. This result provides a rigorous explanation for why naive self-training on the full target domain may fail in source-free adaptation. It also indicates that robust objectives developed under the bounded-noise premise may lose their effectiveness once the pseudo-labels are dominated by systematic target-side bias rather than random label corruption [19, 20].

Although Theorem 1 reveals a genuine failure mode of source-free adaptation, it is derived under a highly structured global-shift model and analyzes pseudo-label behavior over the entire target domain. These assumptions are stronger than the selective and structure-aware adaptation protocols typically used in SF-GDA. Therefore, before concluding that pseudo-label-based graph adaptation is universally unsafe, it is necessary to examine the scope and limitations of the existing theory.

D. Limitations of Existing Theory

Although Theorem 1 reveals a genuine failure mode of source-free adaptation, its conclusion should be interpreted with caution when transferred to source-free graph domain adaptation. The theorem establishes an impossibility result for

a highly structured worst-case regime, whereas practical SF-GDA is conducted under selective adaptation protocols rather than full-domain self-training [15–17, 20].

First, the existing analysis assumes a class-invariant global translation model,

$$x \mid y = k \sim \mathcal{N}(\mu_k + \Delta, \sigma^2 I_d), \quad k \in \{1, 2\},$$

where all classes share the same shift vector Δ . This particular structure is crucial for constructing the mislabeling area in which the source decision boundary becomes systematically misaligned with the target distribution. In realistic graph adaptation scenarios, domain shift is often heterogeneous across classes and intertwined with variations in graph size, sub-structure composition, connectivity patterns, and neighborhood statistics [7, 15, 16].

Second, the theorem requires that the projected shift magnitude

$$\alpha = \frac{\Delta^\top (\mu_2 - \mu_1)}{\|\mu_2 - \mu_1\|^2}$$

be sufficiently large to guarantee that the conditional error on the mislabeling area approaches one. This requirement characterizes a severe and highly directional domain discrepancy. When the shift is moderate, or when Δ is largely orthogonal to the class-separation direction, the condition for near-certain mislabeling is no longer satisfied [20].

Third, and most importantly for SF-GDA, the unbounded-noise theorem analyzes pseudo-label behavior over the entire target domain. In contrast, practical SF-GDA methods rarely update the model using all target samples uniformly. Instead, they typically rely on confidence screening, neighborhood verification, topology-aware refinement, or consistency regularization to restrict training to a filtered subset of target samples that is more likely to provide trustworthy supervision [15–17]. In graph domains, this distinction is particularly consequential because local topology provides additional relational evidence that can either support or invalidate a pseudo-label. As a result, the effective adaptation distribution is often a restricted subset of \mathcal{X}_T , rather than the full target space analyzed by Theorem 1.

Taken together, these observations suggest that the existing unbounded-noise theory should be viewed as a valid characterization of full-domain source-free self-training under strong global-shift assumptions. It does not rule out the possibility that pseudo-label noise becomes bounded on a carefully filtered target subset whose samples satisfy both high prediction confidence and local structural consistency. Therefore, the more relevant theoretical question for SF-GDA is not whether pseudo-label noise is bounded everywhere on \mathcal{X}_T , but whether one can identify a confidence-consistent safe subspace $\mathcal{H}_{\tau, \rho} \subseteq \mathcal{X}_T$ on which the bounded-noise condition is restored.

E. Safe Subspace and Bounded Pseudo-Label Noise

Motivated by the above discussion, we now analyze a restricted adaptation protocol that operates on target samples supported by both source confidence and local structural agreement. Let

$$s(x) = \max_{c \in \mathcal{Y}} p_S(c \mid x), \quad \tilde{y}(x) = \arg \max_{c \in \mathcal{Y}} p_S(c \mid x)$$

denote the source confidence and the corresponding pseudo-label. Let $\mathcal{N}(x)$ be the local neighborhood of x in the target representation space. We define the confidence-qualified consistent neighborhood of x as

$$\mathcal{N}_{\text{same}}^\tau(x) = \{x' \in \mathcal{N}(x) \mid \tilde{y}(x') = \tilde{y}(x), s(x') \geq \tau\}.$$

The corresponding confidence-consistency ratio is

$$r_\tau(x) = \frac{|\mathcal{N}_{\text{same}}^\tau(x)|}{|\mathcal{N}(x)|},$$

and the average radius of the confidence-qualified consistent neighborhood is

$$\bar{r}(x) = \frac{1}{|\mathcal{N}_{\text{same}}^\tau(x)|} \sum_{x' \in \mathcal{N}_{\text{same}}^\tau(x)} d(x, x'),$$

where $d(\cdot, \cdot)$ denotes the metric in the target representation space. If $\mathcal{N}_{\text{same}}^\tau(x) = \emptyset$, we set $\bar{r}(x) = +\infty$.

Definition 1 (Confidence-Consistent Safe Subspace). Given thresholds $\tau \in (0, 1)$ and $\rho \in (0, 1]$, the safe subspace is

$$\mathcal{H}_{\tau, \rho} = \{x \in \mathcal{X}_T \mid s(x) \geq \tau, r_\tau(x) \geq \rho\}. \quad (1)$$

Thus, $\mathcal{H}_{\tau, \rho}$ contains target samples whose pseudo-labels are supported by both source confidence and local neighborhood agreement. The threshold τ controls the population reliability of a selected pseudo-label, while ρ is an observable target-only certificate that prevents isolated high-confidence samples from dominating adaptation.

To analyze the noise behavior inside $\mathcal{H}_{\tau, \rho}$, we use the following two assumptions.

Assumption 1 (Restricted Posterior Discrepancy). For a confidence threshold τ , there exists $\beta_\tau(\alpha) \geq 0$ such that every confidence-qualified target point z satisfies

$$p_T(\tilde{y}(z) \mid z) \geq p_S(\tilde{y}(z) \mid z) - \beta_\tau(\alpha).$$

Here, α denotes the severity of the source-target shift, and $\beta_\tau(\alpha)$ summarizes the residual posterior mismatch on the confidence-qualified region. This assumption is explicitly local to the selected region. Without some target-side posterior regularity of this form, no source-free method can certify pseudo-label correctness from unlabeled target samples alone. **Assumption 2 (Target-Manifold Smoothness).** The target posterior is L -Lipschitz continuous on \mathcal{X}_T :

$$|p_T(y \mid x) - p_T(y \mid x')| \leq Ld(x, x'), \quad \forall x, x' \in \mathcal{X}_T, y \in \mathcal{Y}.$$

The following theorem gives a bounded-noise guarantee on the safe subspace and clarifies the respective roles of confidence, posterior discrepancy, neighborhood consistency, and geometry.

Theorem 2 (Bounded Pseudo-Label Noise in the Safe Subspace). Suppose Assumptions 1 and 2 hold. For every $x \in \mathcal{H}_{\tau, \rho}$, the instance-wise pseudo-label noise satisfies

$$\eta(x) \leq 1 - \tau + \beta_\tau(\alpha). \quad (2)$$

Moreover, the confidence-qualified consistent neighborhood provides the following structural certificates:

$$\frac{1}{|\mathcal{N}(x)|} \sum_{x' \in \mathcal{N}(x)} p_T(\tilde{y}(x) \mid x') \geq \rho(\tau - \beta_\tau(\alpha)), \quad (3)$$

$$p_T(\tilde{y}(x) | x) \geq \tau - \beta_\tau(\alpha) - L\bar{r}(x). \quad (4)$$

Consequently, if $\tau - \beta_\tau(\alpha) > 1/2$, then pseudo-labels on $\mathcal{H}_{\tau,\rho}$ satisfy the Massart bounded-noise condition.

Theorem 2 should be read as a selective rather than global guarantee. The pointwise part follows from high source confidence and restricted posterior discrepancy; its role is not to claim global correctness of pseudo-labels, but to identify the condition under which hard pseudo-label supervision is justified on a selected target subset. It does not contradict the full-domain unbounded-noise result in Theorem 1. The structural quantities ρ and $L\bar{r}(x)$ should not be interpreted as artificially multiplying the pointwise posterior lower bound. Their role is to provide target-only evidence for identifying reliable samples and to prevent adaptation from relying on isolated high-confidence predictions.

Proposition 1 (Finite-Sample Reliability of the Structural Gate). *For a fixed target graph representation x , suppose its k_{nn} neighbors are sampled from the local target-neighborhood distribution, and let $\hat{r}_\tau(x)$ be the empirical confidence-consistency ratio computed from these neighbors. Let $r_\tau(x) = \mathbb{E}[\hat{r}_\tau(x)]$ be the corresponding population ratio. Then, for any $\epsilon > 0$, with probability at least $1 - \delta$,*

$$|\hat{r}_\tau(x) - r_\tau(x)| \leq \sqrt{\frac{\log(2/\delta)}{2k_{\text{nn}}}}. \quad (5)$$

Consequently, if $\hat{r}_\tau(x) \geq \rho_{\min} + \epsilon$ and $k_{\text{nn}} \geq \log(2/\delta)/(2\epsilon^2)$, then $r_\tau(x) \geq \rho_{\min}$ with probability at least $1 - \delta$.

Proof. The empirical ratio $\hat{r}_\tau(x)$ is an average of k_{nn} Bernoulli indicators specifying whether a neighbor has the same pseudo-label and confidence at least τ . Hoeffding's inequality gives Eq. (5). The second statement follows by subtracting the concentration radius from $\hat{r}_\tau(x)$.

F. Learnability and Target-Risk Implications

Theorem 2 becomes algorithmically meaningful when the pseudo-label noise inside the safe subspace falls into a learnable regime. Let

$$\bar{\eta}_\tau = \min\{1, 1 - \tau + \beta_\tau(\alpha)\}.$$

By Theorem 2, $\bar{\eta}_\tau$ is a uniform upper bound of the instance-wise pseudo-label noise on $\mathcal{H}_{\tau,\rho}$.

Corollary 1 (Learnability on the Safe Subspace). *If*

$$\tau - \beta_\tau(\alpha) > \frac{1}{2}, \quad (6)$$

then $\bar{\eta}_\tau < 1/2$, and the pseudo-labels on $\mathcal{H}_{\tau,\rho}$ lie in the bounded-noise regime. Consequently, minimizing a classification-calibrated loss on pseudo-labeled samples from $\mathcal{H}_{\tau,\rho}$ remains statistically learnable under standard noisy-label learning arguments [42, 43].

Corollary 1 shows that reliable source-free adaptation does not require pseudo-label noise to be bounded everywhere on the target domain. It is sufficient that the bounded-noise condition holds on the confidence-consistent subset that actually

drives hard pseudo-label supervision. The size of this subset, controlled in practice by ρ , determines the coverage of reliable supervision and creates a quality-coverage trade-off.

The above bound can be improved in practice when pseudo-labels are produced by a diverse committee rather than a single source model. The following result formalizes the idealized case and also states its limitation.

Corollary 2 (Multi-Expert Voting Bound). *Suppose that the pseudo-label for each $x \in \mathcal{H}_{\tau,\rho}$ is produced by majority voting among K_e conditionally independent experts, each having error at most $\bar{e} < 1/2$ on $\mathcal{H}_{\tau,\rho}$. Then the voting error satisfies*

$$\eta_{\text{vote}}(x) \leq \exp\left(-2K_e \left(\frac{1}{2} - \bar{e}\right)^2\right), \quad \forall x \in \mathcal{H}_{\tau,\rho}. \quad (7)$$

The conditional-independence assumption in Corollary 2 is an idealization. In implementation, source experts trained from the same source domain may be correlated. Therefore, we do not rely on Eq. (7) as an unconditional guarantee. Instead, the algorithm uses ensemble consensus and predictive variance as observable diagnostics: only samples with high agreement and low variance are admitted into the semantic candidate set before structural verification.

Beyond learnability, the safe-subspace view yields a simple target-risk decomposition. Let

$$\pi_{\mathcal{H}} = \Pr_{x \sim P_T} [x \in \mathcal{H}_{\tau,\rho}], \quad \pi_{\mathcal{U}} = 1 - \pi_{\mathcal{H}},$$

where $\mathcal{U} = \mathcal{X}_T \setminus \mathcal{H}_{\tau,\rho}$ denotes the uncertain set. Define the pseudo-label risk on the safe subspace as

$$\tilde{R}_{\mathcal{H}}(h) = \Pr_{x \sim P_T} [h(x) \neq \tilde{y}(x) | x \in \mathcal{H}_{\tau,\rho}],$$

and the clean conditional risk on the uncertain set as

$$R_{\mathcal{U}}(h) = \Pr_{(x,y) \sim P_T} [h(x) \neq y | x \in \mathcal{U}].$$

Proposition 2 (Target-Risk Bound Under Safe-Subspace Decomposition). *For any classifier h , the target risk satisfies*

$$R_T(h) \leq \pi_{\mathcal{H}} \left(\tilde{R}_{\mathcal{H}}(h) + \bar{\eta}_\tau \right) + \pi_{\mathcal{U}} R_{\mathcal{U}}(h). \quad (8)$$

Furthermore, if the uncertain-set risk is controlled by a regularizer-induced upper bound $R_{\mathcal{U}}(h) \leq \Gamma_{\mathcal{U}}(h)$, then

$$R_T(h) \leq \pi_{\mathcal{H}} \left(\tilde{R}_{\mathcal{H}}(h) + \bar{\eta}_\tau \right) + \pi_{\mathcal{U}} \Gamma_{\mathcal{U}}(h). \quad (9)$$

Proof. Decompose the target risk over $\mathcal{H}_{\tau,\rho}$ and \mathcal{U} . On $\mathcal{H}_{\tau,\rho}$, the event $h(x) \neq y$ is contained in the union of the events $h(x) \neq \tilde{y}(x)$ and $\tilde{y}(x) \neq y$. Taking conditional probabilities and using the bound $\Pr[\tilde{y}(x) \neq y | x \in \mathcal{H}_{\tau,\rho}] \leq \bar{\eta}_\tau$ gives Eq. (8). Replacing $R_{\mathcal{U}}(h)$ by its regularized upper bound gives Eq. (9).

Proposition 2 reveals that the target risk is governed by three factors: the fitting error to reliable pseudo-labels on $\mathcal{H}_{\tau,\rho}$, the intrinsic pseudo-label noise level $\bar{\eta}_\tau$ of the safe subspace, and the residual risk on the uncertain set \mathcal{U} . This result directly motivates the use of hard pseudo-label supervision only on $\mathcal{H}_{\tau,\rho}$, while controlling uncertain samples through soft regularization rather than discarding them or assigning hard labels.

G. Roles of the Bounding and Certification Factors

The preceding analysis identifies four quantities: confidence τ , restricted posterior discrepancy $\beta_\tau(\alpha)$, neighborhood consistency ρ , and geometric compactness $L\bar{r}$. Their roles are different. The population noise bound in Eq. (2) is determined by τ and $\beta_\tau(\alpha)$: if confidence is low or the source-target posterior discrepancy is large, no bounded-noise guarantee can be obtained. By contrast, ρ and $L\bar{r}$ are target-only certification factors. They do not create correctness by themselves; rather, they improve the reliability of the selected subset by excluding isolated high-confidence predictions and by ensuring that local neighborhood evidence is geometrically meaningful.

This distinction is important for a rigorous interpretation of the theory. We do not claim that all four quantities are mathematically necessary for a pointwise posterior bound once high source confidence and restricted posterior discrepancy already hold at the center point. Instead, we use ρ and $L\bar{r}$ to bridge the gap between population assumptions and a practical label-free algorithm: they determine which target samples are sufficiently supported by the learned target manifold to be used for hard pseudo-label training.

H. Implications for Algorithm Design

The theoretical analysis prescribes the following design principles. First, the algorithm should increase the reliability of source-induced pseudo-labels by selecting high-confidence, low-variance predictions, corresponding to the terms τ and $\beta_\tau(\alpha)$. Second, it should learn a compact and smooth target representation so that neighborhood evidence is meaningful, corresponding to the geometric term $L\bar{r}$. Third, it should enforce a local consistency gate ρ to avoid isolated overconfident errors. Fourth, it should handle the residual uncertain set \mathcal{U} through soft regularization, as required by Proposition 2.

Guided by this correspondence, we develop in the next section a selective-risk-guided SF-GDA framework with four modules. The first module uses a committee of source experts to construct reliable semantic candidates with high consensus and low predictive variance. The second module learns a target-intrinsic structural manifold to reduce geometric distortion and improve local smoothness. The third module identifies the safe subspace $\mathcal{H}_{\tau,\rho}$ by enforcing consistency between semantic confidence and structural neighborhoods. The fourth module handles the remaining uncertain samples through soft regularization, thereby controlling residual transfer risk without propagating erroneous hard pseudo-labels.

IV. METHODOLOGY

A. Overview

Motivated by the selective-risk analysis in Section III-H, we propose Safe-Subspace Pseudo-Label Refinement (S²PLR) for source-free graph domain adaptation. The framework follows a simple principle: hard pseudo-label supervision is used only on target graphs that pass both semantic and structural reliability checks, while the remaining target graphs are exploited through soft regularization. This design avoids full-domain self-training and directly matches the safe-subspace decomposition in Proposition 2. Operationally, S²PLR implements

this principle through multi-expert uncertainty quantification, target-intrinsic structure learning, dual-view nested pseudo-label refinement, and noise-tolerated regularization.

Let $\mathcal{D}^t = \{G_j^t\}_{j=1}^{n_t}$ be the unlabeled target set. The source provider releases a committee of K_e pretrained source hypotheses $\mathcal{M} = \{f_S^k\}_{k=1}^{K_e}$, which may be obtained from different random seeds or heterogeneous graph encoders before the source data are discarded. During target adaptation, no source graph or source label is accessed. In the algorithmic implementation, ζ is the empirical counterpart of the theoretical confidence threshold τ , and ρ_{\min} is the empirical neighborhood-consistency threshold used to construct $\mathcal{H}_{\zeta,\rho}$. Unless otherwise stated, the adapted target classifier f_T is initialized from a primary source checkpoint and is the only model used at inference; auxiliary source experts are frozen and used only for reliability estimation. When $K_e = 1$, S²PLR reduces to a single-expert variant by disabling the ensemble-variance gate.

B. Module I: Multi-Expert Uncertainty Quantification

Corollary 2 motivates the use of a diverse source committee, while also making clear that correlated experts cannot be treated as independent without verification. We therefore use the committee not only to average predictions but also to estimate predictive disagreement. For a target graph G_j^t , the ensemble consensus is

$$\bar{p}_j = \frac{1}{K_e} \sum_{k=1}^{K_e} \sigma(f_S^k(G_j^t)), \quad (10)$$

where $\sigma(\cdot)$ denotes the softmax function. The corresponding pseudo-label and confidence are

$$\hat{y}_j = \arg \max_{c \in \mathcal{Y}} \bar{p}_{j,c}, \quad s_j = \max_{c \in \mathcal{Y}} \bar{p}_{j,c}.$$

To reject samples whose apparent confidence is caused by one unstable expert rather than shared semantic evidence, we compute the predictive variance

$$u_j = \frac{1}{K_e} \sum_{k=1}^{K_e} \|\sigma(f_S^k(G_j^t)) - \bar{p}_j\|_2^2. \quad (11)$$

The semantic candidate set is then defined as

$$\mathcal{S}_{\text{sem}} = \{G_j^t \in \mathcal{D}^t \mid s_j \geq \zeta, u_j \leq \nu\}, \quad (12)$$

where ζ is the confidence threshold and ν is the variance threshold. We set ν by a target-side percentile rule, $\nu = Q_{q_u}(\{u_j\}_{j=1}^{n_t})$, where Q_{q_u} is the q_u -th percentile of predictive variance on the unlabeled target set. This rule is label-free and avoids tuning ν with target labels. This module operationalizes the confidence requirement in Theorem 2; only high-confidence and low-disagreement target graphs are allowed to enter the next verification stage.

C. Module II: Target-Intrinsic Structure Learning

The structural certificates in Theorem 2 require a target representation in which neighborhoods are meaningful and compact. Directly using the source feature space may be

unreliable because the source encoder can preserve source-specific topology. We therefore introduce a target-intrinsic explicit branch g_ψ , trained only with unlabeled target graphs, to provide the metric space used for neighborhood verification.

For each mini-batch \mathcal{B} , we generate two stochastic graph views $\tilde{G}_i^1, \tilde{G}_i^2 \sim \mathcal{T}(G_i)$ using edge dropping, feature masking, and subgraph sampling. Their normalized embeddings are

$$z_i^v = \frac{g_\psi(\tilde{G}_i^v)}{\|g_\psi(\tilde{G}_i^v)\|_2}, \quad v \in \{1, 2\}. \quad (13)$$

We train g_ψ with the graph contrastive objective

$$D_i^v = \sum_{m=1}^{|\mathcal{B}|} \sum_{w=1}^2 \mathbb{I}[(m, w) \neq (i, v)] \exp\left(\frac{\text{sim}(z_i^v, z_m^w)}{\tau_g}\right),$$

$$\mathcal{L}_{\text{GCL}} = -\frac{1}{2|\mathcal{B}|} \sum_{i=1}^{|\mathcal{B}|} \sum_{v=1}^2 \log \frac{\exp(\text{sim}(z_i^v, z_i^{3-v})/\tau_g)}{D_i^v}. \quad (14)$$

Here, D_i^v denotes the contrastive normalization term for anchor z_i^v . By pulling augmented views of the same graph together and separating different graphs, this branch reduces local dispersion and improves the practical reliability of the neighborhood radius \bar{r} used in the safe-subspace construction.

D. Module III: Dual-View Nested Pseudo-Label Refinement

Module I provides a semantic view from the source committee, whereas Module II provides a structural view from the target-intrinsic manifold. The nested refinement module intersects these two views to identify the empirical safe subspace. Specifically, we build a k_{nn} -nearest-neighbor graph in the embedding space produced by g_ψ . For each candidate $G_j^t \in \mathcal{S}_{\text{sem}}$, let \mathcal{N}_j be its k_{nn} nearest target graphs. We compute the local confidence-consistency score

$$\rho_j = \frac{1}{|\mathcal{N}_j|} \sum_{G_i^t \in \mathcal{N}_j} \mathbb{I}[\hat{y}_i = \hat{y}_j, s_i \geq \zeta, u_i \leq \nu]. \quad (15)$$

The safe subspace used for hard pseudo-label supervision is

$$\mathcal{H}_{\zeta, \rho} = \{G_j^t \in \mathcal{S}_{\text{sem}} \mid \rho_j \geq \rho_{\min}\}, \quad (16)$$

and the uncertain set is $\mathcal{U} = \mathcal{D}^t \setminus \mathcal{H}_{\zeta, \rho}$. This selection rule implements the safe-subspace definition at the sample level and is supported by the finite-sample concentration result in Proposition 1. It does not assume that neighborhood consistency alone proves correctness; rather, it uses local consistency as a target-only certificate that screens out isolated high-confidence predictions before they influence model updates.

E. Module IV: Noise-Tolerated Regularization

The uncertain set \mathcal{U} still contains useful information about the target distribution, but Theorem 2 does not justify assigning hard pseudo-labels to these samples. We therefore regularize them softly. Let f_T be the target model initialized from the primary source checkpoint, while auxiliary experts remain frozen for reliability estimation, and let

$$p_j = \sigma(f_T(G_j^t)) \quad (17)$$

be its current target prediction. For uncertain samples, we minimize

$$\mathcal{L}_{\text{reg}} = \frac{1}{|\mathcal{U}|} \sum_{G_j^t \in \mathcal{U}} [\mathcal{H}(p_j) + \lambda_{\text{kl}} D_{\text{KL}}(\text{sg}(\bar{p}_j) \| p_j)], \quad (18)$$

where $\mathcal{H}(\cdot)$ denotes entropy, D_{KL} is the Kullback-Leibler divergence, and $\text{sg}(\cdot)$ stops gradients through the source ensemble anchor. The entropy term encourages low-density decision boundaries on the target domain, while the KL term prevents the target model from drifting arbitrarily far from source knowledge. Since no hard label is imposed on \mathcal{U} , this module controls the residual term $\Gamma_{\mathcal{U}}(h)$ in Proposition 2 without propagating unverified pseudo-label errors.

F. Overall Optimization and Training Protocol

For a mini-batch $\mathcal{B} \subset \mathcal{D}^t$, define $\mathcal{B}_{\mathcal{H}} = \mathcal{B} \cap \mathcal{H}_{\zeta, \rho}$ and $\mathcal{B}_{\mathcal{U}} = \mathcal{B} \cap \mathcal{U}$. The hard-supervision loss on the safe subspace is

$$\mathcal{L}_{\mathcal{H}} = \frac{1}{|\mathcal{B}_{\mathcal{H}}|} \sum_{G_j^t \in \mathcal{B}_{\mathcal{H}}} \mathcal{L}_{\text{ce}}(p_j, \hat{y}_j), \quad (19)$$

with $\mathcal{L}_{\mathcal{H}} = 0$ when $\mathcal{B}_{\mathcal{H}}$ is empty. The total objective is

$$\mathcal{L}_{\text{total}} = \mathcal{L}_{\mathcal{H}} + \lambda_{\text{reg}} \mathcal{L}_{\text{reg}}(\mathcal{B}_{\mathcal{U}}) + \lambda_{\text{struct}} \mathcal{L}_{\text{GCL}}(\mathcal{B}). \quad (20)$$

We optimize Eq. (20) in an alternating manner. At the beginning of each epoch, S²PLR updates ensemble predictions, target structural embeddings, nearest-neighbor relations, and the safe subspace. It then updates f_T and g_ψ using mini-batch stochastic optimization. The details of the algorithm are introduced in Algorithm 1.

G. Complexity Analysis

The additional cost of S²PLR comes from ensemble inference, target contrastive learning, and nearest-neighbor construction. Ensemble inference for reliability estimation costs $\mathcal{O}(K_{\text{ent}} n_t C)$ after the forward representations are computed, where C is the number of classes. Unless an ensemble variant is explicitly reported, test-time prediction uses only the adapted target model f_T , so the default inference cost is that of a single graph classifier. Exact nearest-neighbor construction in a d -dimensional embedding space costs $\mathcal{O}(n_t^2 d)$, and can be replaced by approximate search for large target sets. The contrastive branch has the same order of graph encoder cost as a standard GNN forward pass on augmented views. Since source graphs are never loaded during adaptation, the memory cost is dominated by target mini-batches, cached target embeddings, and the released source checkpoints.

V. EXPERIMENTS

A. Experimental Settings

Datasets. We evaluate S²PLR on image-derived graph benchmarks, i.e., MNIST [44] and CIFAR10 [45], and real-world graph benchmarks from TUDataset¹ and OGB². Following [8, 16, 46], we consider two types of domain shifts.

¹<https://chrsmrrs.github.io/datasets/>

²<https://ogb.stanford.edu/>

TABLE I: Graph classification results (in %) under node and edge density domain shifts on Mutagenicity, and feature domain shifts on DD, PROTEINS, BZR, BZR_MD, COX2, and COX2_MD. For convenience, PROTEINS, DD, COX2, COX2_MD, BZR, and BZR_MD are abbreviated as P, D, C, CM, B, and BM, respectively. **Bold** results indicate the best performance.

Methods	Node Shift			Edge Shift			Feature Shift					
	M0→M1	M0→M2	M0→M3	M0→M1	M0→M2	M0→M3	P→D	D→P	C→CM	CM→C	B→BM	BM→B
WL subtree	34.3	40.4	52.7	34.4	47.6	52.7	43.0	42.2	53.1	58.2	51.3	44.0
GCN	64.1±1.4	65.5±2.0	56.9±2.1	66.3±1.7	63.6±1.4	56.0±1.4	48.9±2.0	60.9±2.3	51.0±1.8	66.9±1.8	48.7±2.0	78.8±1.7
GIN	66.5±2.1	52.0±1.7	53.7±1.7	67.1±1.7	54.2±2.6	55.4±1.9	57.3±2.2	61.9±1.9	53.8±2.5	55.6±2.0	49.9±2.4	79.2±2.8
GMT	65.7±1.8	62.1±2.1	59.0±2.0	67.9±1.3	61.5±1.8	58.2±2.4	59.5±2.5	50.7±2.2	49.3±1.8	58.2±2.0	50.2±2.3	74.4±1.8
CIN	65.1±1.7	66.0±1.7	55.2±1.5	66.3±1.8	60.8±1.7	55.8±2.4	59.1±2.6	58.0±2.7	51.2±2.0	55.6±1.5	49.2±1.4	74.2±1.9
PathNN	70.2±1.5	67.1±2.0	58.0±1.9	68.9±1.9	62.9±1.7	58.1±1.6	57.9±1.8	53.8±3.3	49.8±1.7	66.9±2.5	50.3±2.3	75.3±2.2
SFDA_LLN	70.7±1.6	68.1±1.2	60.4±1.3	67.7±1.5	66.5±2.6	58.8±2.1	59.2±1.1	59.9±1.5	56.9±1.9	74.2±2.0	53.5±2.2	77.3±1.8
SF(DA) ²	72.0±1.5	69.7±1.9	62.0±1.8	71.7±1.9	68.8±2.3	61.9±2.0	62.2±1.7	63.2±1.8	51.7±2.3	74.6±2.6	48.9±1.4	78.8±2.0
NVC_LLN	71.4±1.3	67.8±1.1	62.1±1.5	70.4±2.2	67.0±2.2	62.2±1.7	59.2±2.1	60.0±1.8	56.6±3.1	76.7±2.0	53.8±1.8	78.2±2.0
Ucon_SFDA	73.2±0.8	69.6±2.1	62.9±3.2	74.1±1.1	68.2±1.2	63.5±3.7	64.3±0.7	66.0±2.1	51.2±1.9	78.3±1.7	53.1±2.5	77.9±2.0
SOGA	73.5±1.3	69.4±2.5	63.1±2.1	72.3±2.2	69.8±1.9	63.1±1.8	64.4±1.3	65.4±1.8	51.5±2.0	76.9±2.5	53.3±3.2	78.9±2.3
GraphCTA	73.7±1.8	70.7±1.5	65.2±1.7	72.0±2.2	70.5±1.6	62.8±1.8	60.6±1.9	61.7±1.8	56.8±3.5	77.3±2.0	54.2±2.7	79.0±2.6
GALA	75.1±2.1	70.8±1.6	64.0±2.1	72.2±1.2	70.3±1.7	63.4±1.8	65.6±1.3	66.0±2.5	61.8±2.7	77.0±2.6	57.4±2.3	78.8±1.8
GraphATA	75.2±2.1	69.9±1.3	62.1±1.0	74.4±1.3	69.0±0.9	61.9±2.2	64.8±1.5	63.7±2.1	59.2±2.0	77.9±2.1	55.1±1.3	78.0±3.6
S ² PLR	77.1±0.5	71.6±2.0	65.8±1.1	75.8±2.1	69.9±1.6	66.2±1.4	66.3±1.9	61.8±2.2	59.1±1.5	78.6±0.9	58.3±1.8	79.3±0.8

TABLE II: Image classification results (in %) on MNIST and CIFAR-10 under edge density domain shifts. **Bold** results indicate the best performance.

Methods	MNIST						CIFAR-10					
	S0→S1	S1→S0	S0→S2	S2→S0	S1→S2	S2→S1	C0→C1	C1→C0	C0→C2	C2→C0	C1→C2	C2→C1
WL subtree	29.5	15.8	9.5	8.7	18.0	13.9	10.1	10.2	9.9	10.0	9.9	10.2
GCN	82.4±0.3	84.7±0.3	60.9±1.9	70.5±4.0	81.5±1.0	83.2±0.9	44.9±0.4	46.5±0.2	42.0±1.2	43.0±1.8	44.1±0.3	45.2±0.3
GIN	86.2±1.5	79.8±2.3	81.4±2.6	83.9±2.1	83.2±1.6	84.8±2.2	44.4±2.2	43.1±1.1	43.3±2.1	44.7±1.7	42.4±1.1	42.0±2.8
GMT	83.3±1.3	83.5±1.4	58.2±0.8	68.3±2.4	80.9±1.4	84.6±1.1	52.2±0.4	53.6±0.1	44.1±2.7	50.0±7.6	49.6±0.7	50.0±0.9
CIN	85.8±2.0	86.4±1.8	82.2±1.5	82.8±1.5	86.5±1.7	86.3±2.3	51.0±0.5	55.4±1.9	48.1±3.0	51.9±0.8	47.1±0.4	47.2±0.6
PathNN	80.2±2.8	87.9±1.4	39.3±2.0	53.7±1.6	79.9±1.7	89.6±2.5	43.7±2.0	46.5±1.5	47.6±2.3	52.1±1.6	44.5±2.1	47.7±2.0
SFDA_LLN	93.3±0.3	92.6±1.5	89.7±4.1	88.3±2.0	92.7±1.5	92.1±1.3	56.5±3.4	55.4±1.2	55.2±2.0	53.8±1.5	58.1±0.9	56.7±1.5
SF(DA) ²	93.7±1.0	93.8±1.3	90.6±0.7	90.1±1.3	93.1±1.2	93.3±1.1	56.7±1.4	56.4±1.3	55.1±0.8	53.3±1.4	57.7±1.4	57.4±1.8
NVC_LLN	93.4±1.3	93.2±1.0	88.9±4.8	83.0±1.9	93.2±1.2	92.4±1.5	56.9±1.5	55.9±1.2	55.5±1.4	54.1±2.8	57.8±1.3	57.8±1.0
Ucon_SFDA	93.8±1.7	93.8±0.8	88.5±0.9	90.9±2.2	92.9±0.7	93.8±1.4	57.3±1.7	56.1±2.2	56.6±1.6	54.4±1.5	58.3±0.8	57.5±1.3
SOGA	93.9±1.1	94.3±1.7	91.5±1.3	90.1±2.0	93.2±1.1	93.8±1.0	57.6±1.1	57.0±1.3	56.3±1.7	56.8±1.4	57.9±0.9	58.1±2.2
GraphCTA	93.8±1.0	94.5±2.1	91.1±0.9	88.2±1.7	94.1±2.0	93.5±1.4	57.9±0.9	57.4±0.8	57.0±1.5	56.7±2.2	57.7±1.1	58.4±1.3
GALA	94.1±1.7	94.9±0.9	91.8±1.1	89.2±0.6	93.9±0.8	94.0±0.7	58.1±1.2	57.6±0.8	57.4±0.7	56.9±2.2	58.3±1.3	58.8±1.5
GraphATA	93.2±2.1	94.5±1.0	91.7±1.5	89.5±1.7	93.3±2.2	94.1±0.9	57.2±1.3	56.7±2.8	58.8±1.9	54.4±1.6	59.3±1.7	57.6±2.5
S ² PLR	94.7±1.4	95.8±0.3	92.5±1.3	91.6±1.0	94.3±0.6	94.5±0.8	58.7±1.1	57.8±1.4	56.4±0.7	57.9±2.2	58.0±1.2	59.0±2.0

For structural domain shifts, MNIST, CIFAR10, DD, Mutagenicity, NCI1, FRANKENSTEIN, and ogbg-molhiv are partitioned into quantile-based subdomains according to the number of nodes $|V|$ or edges $|E|$, and each ordered pair of distinct subdomains is treated as a source-free transfer task. For feature domain shifts, we evaluate PROTEINS \leftrightarrow DD, COX2 \leftrightarrow COX2_MD, and BZR \leftrightarrow BZR_MD, where source and target domains share the same label space but differ in node-feature distributions. More details of these datasets are provided in Appendix C.

Baselines. We compare S²PLR with three groups of baselines. The first group consists of source-only graph learning methods, including the graph kernel WL [47] and representative graph neural networks, i.e., GCN [48], GIN [49], CIN [50], GMT [51], and PathNN [52]. These methods are trained on the labeled source domain and directly evaluated on the target domain without source-free adaptation. The second group includes general source-free domain adaptation methods, namely SFDA_LLN [19], SF(DA)² [28], NVC_LLN [20], and Ucon_SFDA [53]. The third group contains graph-specific source-free domain adaptation methods, including SOGA [15], GraphCTA [54], GALA [16], and GraphATA [32]. More

details of baselines are provided in Appendix D.

Implementation Details. We implement S²PLR and all baselines in PyTorch³ and run all experiments on NVIDIA A100 GPUs. Source models are trained only with labeled source graphs, and source graphs and labels are inaccessible during target adaptation. Unless otherwise specified, the target encoder is a 3-layer GNN with hidden dimension 256, optimized by Adam with learning rate 10^{-4} and weight decay 10^{-12} . For S²PLR, we fix $K_e = 3$ source experts for all datasets. All hyperparameters are determined without using target labels, which are used only for final evaluation. We report classification accuracy on image and TUDataset benchmarks, and ROC-AUC on OGB benchmarks. All results are averaged over five independent runs with different random seeds and reported with standard deviation.

B. Performance Comparison

We report the performance of S²PLR and all baselines under the source-free graph domain adaptation setting in Tables I, II, and XVI–XXV. Overall, the results show that source-only

³<https://pytorch.org/>

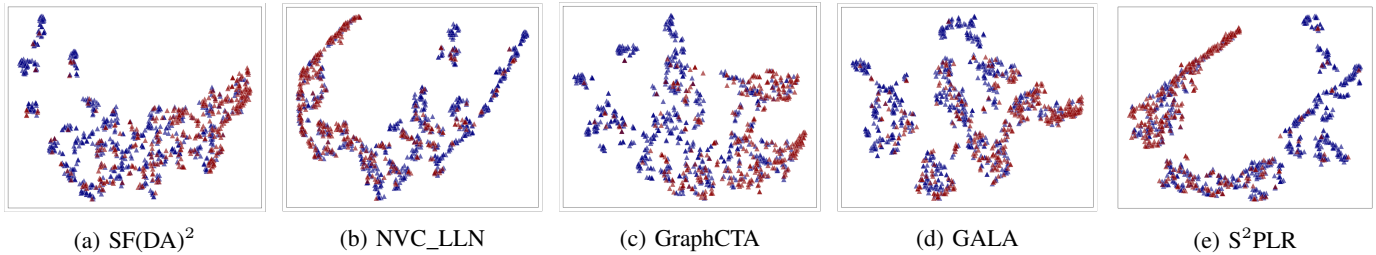


Fig. 1: T-SNE visualizations of S^2 PLR and baselines on the Mutagenicity dataset.

TABLE III: Aggregate comparison across all reported transfer tasks. **Bold** results indicate the best performance.

Method	Node Avg.	Edge Avg.	Overall Avg.	Avg. Rank	S^2 PLR W/T/L
WL	49.29	43.23	46.10	13.60	138/0/0
GCN	51.36	53.39	52.76	12.55	134/4/0
GIN	51.79	54.25	53.42	12.61	134/4/0
GMT	53.62	55.12	54.55	11.97	137/1/0
CIN	51.65	54.83	53.58	12.40	134/4/0
PathNN	56.15	57.32	56.89	11.11	135/3/0
SFDA_LLN	64.67	66.42	65.53	8.01	94/44/0
SF(DA) ²	65.68	67.25	66.39	6.85	89/48/1
NVC_LLN	65.27	66.81	66.02	7.46	90/48/0
Ucon_SFDA	66.11	67.94	67.02	5.75	80/56/2
SOGA	67.08	68.45	67.71	4.91	68/69/1
GraphCTA	67.60	68.69	68.06	4.26	66/71/1
GALA	67.92	69.22	68.59	3.21	63/72/3
GraphATA	68.66	69.88	69.20	3.53	54/80/4
S^2 PLR	71.81	72.77	72.11	1.80	–

graph models, including WL, GCN, GIN, CIN, GMT, and PathNN, often degrade under structural domain shifts because they cannot adapt to the target distribution after source graphs become unavailable. General source-free domain adaptation methods, such as SF(DA)² and Ucon_SFDA, improve over source-only models but remain less stable on graph-structured shifts, as they do not explicitly model graph topology or local structural consistency. Graph-specific adaptation methods, including GALA and GraphATA, provide stronger baselines and can be competitive on some transfer pairs, especially when the shift is mild or pseudo-labels are relatively reliable. In contrast, S^2 PLR achieves the best or empirically comparable performance in most settings. Its advantage comes from jointly using multi-expert semantic reliability estimation, target-intrinsic structural learning, and nested safe-subspace refinement, which restricts hard supervision to reliable target samples while regularizing uncertain ones. We also provide t-SNE visualizations on Mutagenicity in Fig. 1. Compared with baselines, S^2 PLR produces more compact and better separated target representations, whereas the baselines, e.g., NVC_LLN and GALA, show stronger class mixing or scattered local structure. This qualitative evidence is consistent with the quantitative results and suggests that S^2 PLR improves target-domain discriminability under structural shifts. More results on other datasets can be found in Appendix F1.

We further summarize the aggregate results in Table III. Node Avg. and Edge Avg. are computed over the corresponding node-density and edge-density transfer tasks, while Overall Avg. and Avg. Rank are computed over all unique transfer tasks, including feature-shift settings. For W/T/L, S^2 PLR is compared with each baseline on every task using the reported mean \pm standard-deviation intervals, where overlapping inter-

vals are treated as ties. The aggregate results show that S^2 PLR achieves the best performance across Node Avg., Edge Avg., Overall Avg., and Avg. Rank, indicating that its improvements are consistent across diverse domain shifts rather than concentrated on a few favorable tasks. The newly added baselines, especially GraphATA and Ucon_SFDA, further strengthen the comparison and improve over several previous source-free adaptation methods. Nevertheless, S^2 PLR still maintains the strongest overall robustness. The W/T/L statistics also show that S^2 PLR rarely underperforms existing methods, while many comparisons with strong graph adaptation baselines are counted as ties due to overlapping uncertainty intervals. These results further confirm the effectiveness of reliability-guided safe-subspace selection under node-density, edge-density, and feature-domain shifts.

C. Pseudo-Label Quality Diagnostics

Since the core design of S^2 PLR lies in reliable pseudo-label selection, final classification performance alone cannot fully reveal whether the selected target samples are trustworthy. We therefore report post-hoc pseudo-label quality diagnostics in Table IV to directly evaluate the selective-learning mechanism. Candidate Cov. and Candidate Prec. denote the coverage $|\mathcal{S}_{\text{sem}}|/n_t$ and pseudo-label precision of the semantic candidate set, respectively. Safe Cov. and Safe Prec. denote the coverage $|\mathcal{H}_{\zeta,\rho}|/n_t$ and pseudo-label precision of the final safe subspace. We further report Precision Gain and Coverage Drop to quantify how much neighborhood-consistency refinement improves pseudo-label reliability at the cost of reducing selected-sample coverage. Target labels are used only for this post-hoc diagnostic analysis.

The results reveal a consistent precision–coverage trade-off across the reported datasets and shift types. Compared with the initial semantic candidate set, the final safe subspace consistently achieves higher pseudo-label precision, confirming that neighborhood-consistency verification effectively filters out unreliable samples that pass confidence-based semantic selection alone. This improvement is especially evident on structurally shifted graph datasets such as DD, NCI1, and FRANKENSTEIN, where confidence-only pseudo-labels are more vulnerable to topology-induced bias; Mutagenicity also shows clear gains under both node- and edge-density shifts. For ogbg-molhiv and MNIST, the candidate pseudo-labels are already highly reliable, so the additional gain from safe-subspace refinement is relatively smaller but remains positive. CIFAR10 is more challenging, with lower candidate reliability and limited safe coverage, suggesting that conservative

TABLE IV: Post-hoc coverage–precision diagnostics for semantic candidates and the final safe subspace across datasets and shift types.

Dataset	Shift Type	Candidate Cov.	Candidate Prec.	Safe Cov.	Safe Prec.	Precision Gain	Coverage Drop
Mutagenicity	Node	35.06%	86.32%	23.25%	92.46%	+6.14%	11.81%
Mutagenicity	Edge	29.70%	80.43%	15.96%	89.60%	+9.16%	13.75%
NCII	Node	24.34%	77.60%	13.05%	88.06%	+10.46%	11.30%
NCII	Edge	20.25%	82.21%	11.49%	93.22%	+11.01%	8.76%
FRANKENSTEIN	Node	50.00%	68.82%	12.73%	84.06%	+15.24%	37.27%
FRANKENSTEIN	Edge	50.00%	71.96%	12.82%	84.89%	+12.94%	37.18%
DD	Node	50.17%	58.11%	14.92%	70.45%	+12.35%	35.25%
DD	Edge	45.08%	57.89%	10.17%	73.33%	+15.44%	34.92%
ogbg-molhiv	Node	49.97%	97.88%	12.61%	99.15%	+1.27%	37.36%
ogbg-molhiv	Edge	50.00%	97.22%	8.10%	98.92%	+1.70%	41.90%
MNIST	Edge	49.74%	98.04%	20.37%	99.28%	+1.25%	29.37%
CIFAR10	Edge	35.40%	63.71%	10.56%	69.95%	+6.24%	24.84%

TABLE V: Controlled comparison of source-hypothesis budgets among S²PLR and baselines on the Mutagenicity dataset.

Method	Source Hyp.	Committee Type	Trainable Target Models	Test Models	Node Shift			Edge Shift			Avg. Rank
					M0→M1	M0→M2	M0→M3	M0→M1	M0→M2	M0→M3	
GraphATA-Single	1	None	1	1	74.1±1.4	69.3±1.7	59.7±0.9	73.8±1.3	70.0±0.7	60.6±2.5	10.25
GraphATA-Homo3	3	Homogeneous	3	3	74.4±1.8	68.7±2.0	60.1±0.7	74.1±2.3	68.9±0.5	61.6±1.3	10.50
GraphATA-Hetero3	3	Heterogeneous	3	3	75.2±2.1	69.9±1.3	62.1±1.0	74.4±1.3	69.0±0.9	61.9±2.2	8.50
GALA-Single	1	None	1	1	75.1±2.1	70.8±1.6	64.0±2.1	72.2±1.2	70.3±1.7	63.4±1.8	6.00
GALA-Homo3	3	Homogeneous	3	3	75.7±0.1	68.4±0.4	63.1±0.5	73.7±0.2	67.7±2.7	60.3±1.3	10.75
GALA-Hetero3	3	Heterogeneous	3	3	75.7±1.0	70.0±0.6	63.7±2.2	74.7±0.8	69.5±1.5	61.4±1.9	6.67
GraphCTA-Single	1	None	1	1	73.7±1.8	70.7±1.5	65.2±1.7	72.0±2.2	70.5±1.6	62.8±1.8	6.83
GraphCTA-Homo3	3	Homogeneous	3	3	74.5±2.1	67.8±1.3	64.2±1.6	73.9±1.1	67.0±0.8	61.7±1.3	10.42
GraphCTA-Hetero3	3	Heterogeneous	3	3	75.5±1.8	70.1±2.2	63.8±1.4	74.4±1.3	69.0±2.1	62.5±1.8	6.50
SOGA-Single	1	None	1	1	73.5±1.3	69.4±2.5	63.1±2.1	72.3±2.2	69.8±1.9	63.1±1.8	9.25
SOGA-Homo3	3	Homogeneous	3	3	72.8±2.5	67.4±1.1	59.7±0.6	73.3±0.4	68.7±0.5	62.2±0.5	12.58
SOGA-Hetero3	3	Heterogeneous	3	3	75.7±1.1	70.3±0.5	65.5±1.6	74.7±1.8	69.5±1.2	62.0±1.9	4.67
S ² PLR-Single	1	None	1	1	75.3±1.6	67.9±2.3	63.3±1.8	73.7±2.5	67.7±1.3	63.2±1.9	9.33
S ² PLR-Homo3	3	Homogeneous	1	1	76.3±0.1	67.8±3.2	64.7±0.7	74.6±0.4	68.6±1.0	64.8±2.3	6.25
S ² PLR-Hetero3	3	Heterogeneous	1	1	77.1±0.5	71.6±2.0	65.8±1.1	75.8±2.1	69.9±1.6	66.2±1.4	1.50

pseudo-label selection is harder on complex image-derived graphs. Overall, these diagnostics show that S²PLR prioritizes pseudo-label reliability over pseudo-label quantity: it selects a smaller but more trustworthy safe subspace for hard supervision, while leaving uncertain samples to be handled by noise-tolerated regularization.

D. Source-Hypothesis Budget and Committee Design

The source committee in S²PLR is introduced to provide reliable uncertainty signals rather than simply to increase model capacity. To examine the effects of source-hypothesis budget, encoder diversity, and reliability-guided refinement, we report a controlled comparison in Table V. For S²PLR, S²PLR-Single uses one GMT source hypothesis, S²PLR-Homo3 uses three GMT hypotheses trained with different random seeds, and S²PLR-Hetero3 uses a heterogeneous committee composed of GMT, GIN, and PathNN. All three variants use only one trainable target model and one test model, and the released source hypotheses are used only for semantic reliability estimation. For comparison, we apply analogous Single, Homo3, and Hetero3 settings to baselines, including GraphATA, GALA, GraphCTA, and SOGA, where the heterogeneous baseline setting uses GIN, SAGE, and GMT source models.

The results show that increasing the number of source hypotheses alone does not guarantee better adaptation. For

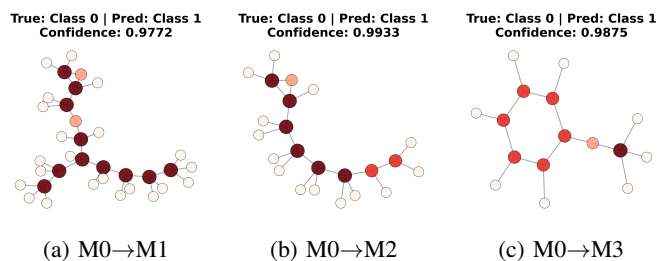


Fig. 2: High-confidence false pseudo-labels on Mutagenicity.

S²PLR, the homogeneous three-GMT committee improves over the single-GMT variant in most transfer tasks, while the heterogeneous GMT/GIN/PathNN committee achieves the best average rank and the strongest overall performance. This indicates that complementary graph encoders provide more informative disagreement signals for identifying reliable pseudo-label candidates. In contrast, the multi-hypothesis variants of GraphATA, GALA, GraphCTA, and SOGA show less consistent improvements, and some Homo3 or Hetero3 variants even underperform their single-model counterparts despite using more trainable target models and test-time models. These observations suggest that the advantage of S²PLR is not merely due to a larger source-hypothesis budget or increased test-time capacity. Rather, the key benefit comes from integrating multi-expert disagreement with target-structural verification

TABLE VI: Per-class safe-subspace diagnostics on the Mutagenicity dataset.

Dataset	Domain	Shift Type	Safe Coverage	Target Distribution		Safe-Subspace Pseudo-labels		Per-Class Safe Prec.	
				Class 0	Class 1	Class 0	Class 1	Class 0	Class 1
Mutagenicity	Node	M0→M1	23.25%	67.34%	32.66%	76.19%	23.81%	94.79%	85.00%
		M0→M2	21.86%	59.87%	40.13%	71.31%	28.69%	89.35%	80.88%
		M0→M3	30.14%	46.73%	53.27%	37.31%	62.69%	76.23%	71.71%
	Edge	M0→M1	29.89%	66.70%	33.30%	75.31%	24.69%	94.67%	86.25%
		M0→M2	15.96%	57.01%	42.99%	56.65%	43.35%	86.73%	93.33%
		M0→M3	18.34%	46.36%	53.64%	46.73%	53.27%	73.12%	76.42%

TABLE VII: The results of ablation studies on the Mutagenicity dataset (source → target).

Methods	M0→M1	M1→M0	M0→M2	M2→M0	M0→M3	M3→M0	M1→M2	M2→M1	M1→M3	M3→M1	M2→M3	M3→M2
S ² PLR w/o ME	76.4	75.1	68.5	73.0	61.1	68.0	77.1	84.3	67.1	79.5	70.4	76.6
S ² PLR w/o CF	76.2	74.0	68.9	74.8	64.7	71.2	79.0	86.2	70.3	80.1	71.3	80.8
S ² PLR w/o TS	76.0	74.5	68.2	73.6	64.6	70.2	78.5	86.0	69.0	79.8	70.7	80.2
S ² PLR w/o NC	76.8	75.4	69.1	74.0	64.8	70.3	78.6	85.7	68.8	80.1	70.5	80.7
S ² PLR w/o SR	74.5	72.5	69.5	73.5	58.8	70.2	76.7	81.8	66.9	75.9	67.5	79.9
S ² PLR	77.1	75.3	71.6	75.4	65.8	72.0	79.9	87.2	70.8	82.4	71.9	81.6

and safe-subspace supervision.

E. Failure Analysis of Safe-Subspace Selection

We further conduct a failure analysis on the Mutagenicity dataset to examine the limitations of safe-subspace selection under severe structural shifts. Table VI reports the target class distribution, the pseudo-label distribution within the selected safe subspace, and the class-wise pseudo-label precision after safe selection. Here, Per-Class Safe Prec. measures the precision of selected safe samples conditioned on each predicted pseudo-label class, and target labels are used only for post-hoc analysis. The results show that the safe subspace is generally reliable under mild or moderate shifts, but its class composition and class-wise reliability may become biased when the structural shift becomes severe. This issue can be further amplified by class-prior variation induced by density-based partitioning, since the selection process may favor the class whose structural patterns are more confidently recognized by the source hypothesis. For example, under the node-density shift M0→M3, the safe pseudo-label distribution becomes more skewed toward Class 1 than the true target distribution, while the class-wise precision also drops. This suggests that some Class-0 target graphs can be absorbed into the Class-1 prediction region, even after confidence-based filtering and neighborhood-consistency verification. For edge-density shifts, the selected class distribution can remain relatively balanced, but class-wise precision still decreases under harder transfers, indicating that class balance alone is insufficient to guarantee pseudo-label correctness.

Additionally, Fig. 2 visualizes representative high-confidence failure cases where Class-0 target graphs are predicted as Class 1. These graphs contain local dense or branched structural patterns that may resemble source-domain Class-1 cues, suggesting that the source hypothesis can rely on shortcut structural signals under topology shift. Such cases explain why aggressive pseudo-label expansion is risky: even highly confident predictions may be systematically wrong in certain target regions. This analysis supports the design of S²PLR, which restricts hard supervision to a verified

safe subspace and handles the remaining uncertain samples through noise-tolerated regularization.

F. Ablation Study

We conduct ablation studies to evaluate the contribution of each component in S²PLR, with variants corresponding to the four modules in Section IV. S²PLR w/o ME removes multi-expert uncertainty quantification and uses a single source hypothesis, disabling the predictive-variance-based disagreement criterion. S²PLR w/o CF removes confidence-based semantic filtering and admits pseudo-labels without the threshold ζ . S²PLR w/o TS removes the target-intrinsic structure learning branch and graph contrastive objective, so neighborhoods are not constructed from a target-specific structural manifold. S²PLR w/o NC removes neighborhood-consistency filtering and disables the structural gate ρ_{\min} . S²PLR w/o SR removes soft regularization on the uncertain set \mathcal{U} , leaving only hard pseudo-label supervision on the safe subspace.

Experimental results are shown in Table VII. The results show that each component contributes to robust adaptation. First, removing ME or CF weakens semantic reliability estimation: the former loses ensemble-disagreement filtering, while the latter admits low-confidence samples, both increasing pseudo-label noise. Second, removing TS degrades performance because the model can no longer learn target-specific structural neighborhoods, making refinement more dependent on source-biased representations. Third, removing NC allows semantic candidates to be used for hard supervision without local structural verification, confirming that confidence alone is insufficient for reliable graph pseudo-labeling. Finally, removing SR underutilizes uncertain target samples, indicating that noise-tolerated regularization helps exploit target distribution information without assigning unreliable hard labels. More results on other datasets are provided in Appendix F2.

G. Sensitivity Analysis

We conduct a sensitivity analysis on two key thresholds in S²PLR, namely the confidence threshold ζ and the neighborhood-consistency threshold ρ_{\min} , as illustrated in

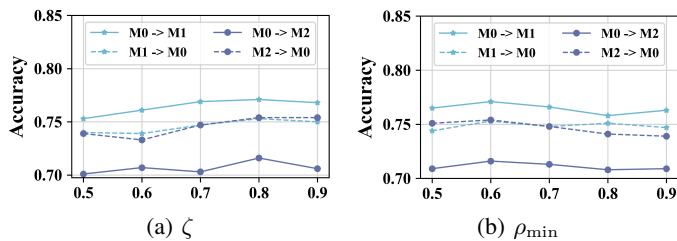


Fig. 3: Sensitivity analysis of the confidence threshold ζ and neighborhood-consistency threshold ρ_{\min} in S^2 PLR on the Mutagenicity dataset.

Fig. 3. The confidence threshold ζ controls the semantic confidence required for selecting pseudo-label candidates, while ρ_{\min} determines the minimum local neighborhood agreement needed for a sample to be admitted into the safe subspace. To evaluate the robustness of S^2 PLR with respect to these thresholds, we vary one parameter at a time while fixing the other hyperparameters to their default settings. Specifically, both ζ and ρ_{\min} are varied over $\{0.5, 0.6, 0.7, 0.8, 0.9\}$.

As shown in Fig. 3, both thresholds exhibit a clear quality-coverage trade-off. For ζ , increasing the threshold generally improves pseudo-label reliability by filtering out low-confidence predictions, but an overly strict threshold may reduce the safe-subspace coverage and limit the amount of hard supervision. On the Mutagenicity dataset, $\zeta = 0.8$ provides a favorable balance between pseudo-label quality and selected-sample coverage. For ρ_{\min} , smaller values may admit locally inconsistent samples into the safe subspace, whereas larger values may discard useful target samples whose neighborhoods are only partially consistent under domain shift. The setting $\rho_{\min} = 0.6$ achieves a stable compromise between structural reliability and effective target coverage. Overall, the results indicate that S^2 PLR is reasonably robust to threshold choices when the semantic and structural filters are set within a moderate range. Additional sensitivity results on other datasets are provided in Appendix F3.

VI. CONCLUSION

This paper revisited source-free graph domain adaptation from the perspective of selective adaptation under systematic pseudo-label noise. Instead of assuming that source-induced pseudo-labels are reliable over the entire target domain, we characterized a confidence-consistent safe subspace where hard pseudo-label supervision can be more cautiously justified. Based on this view, we proposed S^2 PLR, which integrates source-committee uncertainty estimation, target-intrinsic structural representation learning, semantic-structural pseudo-label verification, and noise-tolerant regularization for uncertain target samples. Extensive experiments on image and graph benchmarks under node-density, edge-density, and feature shifts demonstrate that S^2 PLR improves pseudo-label reliability and achieves robust performance across diverse source-free transfer settings. Further diagnostic, ablation, sensitivity, and source-hypothesis budget analyses show that the gains mainly come from reliability-guided safe-subspace supervision rather than simply from additional source hypotheses. A remaining limitation is that safe-subspace selection may become overly

conservative or class-biased under severe structural shifts, suggesting future work on adaptive coverage control and class-aware reliability estimation for broader SF-GDA scenarios.

REFERENCES

- [1] M. Long, Y. Cao, Z. Cao, J. Wang, and M. I. Jordan, “Transferable representation learning with deep adaptation networks,” *IEEE transactions on pattern analysis and machine intelligence*, vol. 41, no. 12, pp. 3071–3085, 2018.
- [2] Z. Wu, S. Pan, F. Chen, G. Long, C. Zhang, and S. Y. Philip, “A comprehensive survey on graph neural networks,” *IEEE Transactions on Neural Networks and Learning Systems*, vol. 32, no. 1, pp. 4–24, 2020.
- [3] Y. Xie, Z. Xu, J. Zhang, Z. Wang, and S. Ji, “Self-supervised learning of graph neural networks: A unified review,” *IEEE transactions on pattern analysis and machine intelligence*, vol. 45, no. 2, pp. 2412–2429, 2022.
- [4] W. Jin, T. Zhao, J. Ding, Y. Liu, J. Tang, and N. Shah, “Empowering graph representation learning with test-time graph transformation,” *arXiv preprint arXiv:2210.03561*, 2022.
- [5] W. Jin, Y. Ma, X. Liu, X. Tang, S. Wang, and J. Tang, “Graph structure learning for robust graph neural networks,” in *Proceedings of the International ACM SIGKDD Conference on Knowledge Discovery & Data Mining*, 2020, pp. 66–74.
- [6] Y. Wang, S. Liu, M. Wang, S. Liang, and N. Yin, “Degree distribution based spiking graph networks for domain adaptation,” *arXiv preprint arXiv:2410.06883*, 2024.
- [7] M. Liu, Z. Zhang, J. Tang, J. Bu, B. He, and S. Zhou, “Revisiting, benchmarking and understanding unsupervised graph domain adaptation,” *Proceedings of the Conference on Neural Information Processing Systems*, vol. 37, pp. 89408–89436, 2024.
- [8] N. Yin, L. Shen, M. Wang, L. Lan, Z. Ma, C. Chen, X.-S. Hua, and X. Luo, “Coco: A coupled contrastive framework for unsupervised domain adaptive graph classification,” in *Proceedings of the International Conference on Machine Learning*, 2023, pp. 40040–40053.
- [9] Y. Wang, K. Zhang, J. Huang, M. Wang, M. Xiao, S. Gao, and N. Yin, “Dsbd: Dual-aligned structural basis distillation for graph domain adaptation,” *arXiv preprint arXiv:2604.03154*, 2026.
- [10] Y. Wang, X. Liu, M. Wang, S. Gao, and N. Yin, “Riemannian flow matching for disentangled graph domain adaptation,” *arXiv preprint arXiv:2602.00656*, 2026.
- [11] J. Li, Z. Yu, Z. Du, L. Zhu, and H. T. Shen, “A comprehensive survey on source-free domain adaptation,” *IEEE Transactions on Pattern Analysis and Machine Intelligence*, vol. 46, no. 8, pp. 5743–5762, 2024.
- [12] D. Zhao, S. Wang, Q. Zang, L. Jiao, N. Sebe, and Z. Zhong, “Stable neighbor denoising for source-free domain adaptive segmentation,” in *Proceedings of the IEEE/CVF Conference on Computer Vision and Pattern Recognition*, 2024, pp. 23416–23427.
- [13] S. Tang, W. Su, M. Ye, and X. Zhu, “Source-free domain adaptation with frozen multimodal foundation model,”

- in *The IEEE/CVF Conference on Computer Vision and Pattern Recognition*, 2024, pp. 23 711–23 720.
- [14] Y. Kim, D. Cho, K. Han, P. Panda, and S. Hong, “Domain adaptation without source data,” *IEEE Transactions on Artificial Intelligence*, vol. 2, no. 6, pp. 508–518, 2021.
- [15] H. Mao, L. Du, Y. Zheng, Q. Fu, Z. Li, X. Chen, S. Han, and D. Zhang, “Source free graph unsupervised domain adaptation,” in *Proceedings of the International ACM Conference on Web Search & Data Mining*, 2024, pp. 520–528.
- [16] J. Luo, Y. Gu, X. Luo, W. Ju, Z. Xiao, Y. Zhao, J. Yuan, and M. Zhang, “Gala: Graph diffusion-based alignment with jigsaw for source-free domain adaptation,” *IEEE Transactions on Pattern Analysis and Machine Intelligence*, vol. 46, no. 12, pp. 9038–9051, 2024.
- [17] J. Luo, Z. Xiao, Y. Wang, X. Luo, J. Yuan, W. Ju, L. Liu, and M. Zhang, “Rank and align: Towards effective source-free graph domain adaptation,” *arXiv preprint arXiv:2408.12185*, 2024.
- [18] Y. Wang, M. Wang, Z. Huang, S. Liu, and N. Yin, “Nested graph pseudo-label refinement for noisy label domain adaptation learning,” in *Proceedings of the AAAI Conference on Artificial Intelligence*, vol. 40, no. 31, 2026, pp. 26 697–26 705.
- [19] L. Yi, G. Xu, P. Xu, J. Li, R. Pu, C. Ling, A. I. McLeod, and B. Wang, “When source-free domain adaptation meets learning with noisy labels,” *arXiv preprint arXiv:2301.13381*, 2023.
- [20] G. Xu, L. Yi, P. Xu, J. Li, R. Pu, C. Shui, C. Ling, A. I. McLeod, and B. Wang, “Unraveling the mysteries of label noise in source-free domain adaptation: Theory and practice,” *IEEE Transactions on Pattern Analysis and Machine Intelligence*, 2025.
- [21] J. Wang, X. Xia, L. Lan, X. Wu, J. Yu, W. Yang, B. Han, and T. Liu, “Tackling noisy labels with network parameter additive decomposition,” *IEEE Transactions on Pattern Analysis and Machine Intelligence*, vol. 46, no. 9, pp. 6341–6354, 2024.
- [22] S. Yang, J. Van de Weijer, L. Herranz, S. Jui *et al.*, “Exploiting the intrinsic neighborhood structure for source-free domain adaptation,” *Advances in neural information processing systems*, vol. 34, pp. 29 393–29 405, 2021.
- [23] J. N. Kundu, N. Venkat, R. V. Babu *et al.*, “Universal source-free domain adaptation,” in *The IEEE/CVF Conference on Computer Vision and Pattern Recognition*, 2020, pp. 4544–4553.
- [24] S. Yang, Y. Wang, J. Van De Weijer, L. Herranz, and S. Jui, “Generalized source-free domain adaptation,” in *The IEEE/CVF Conference on Computer Vision and Pattern Recognition*, 2021, pp. 8978–8987.
- [25] Z. Wen, Q. Li, Y. Wang, H. Shao, and G. Sun, “Fg-plfa: Fine-grained pseudo-labeling and feature alignment for source-free unsupervised domain adaptation,” *IEEE Transactions on Neural Networks and Learning Systems*, 2025.
- [26] S. Qu, T. Zou, L. He, F. Röhrbein, A. Knoll, G. Chen, and C. Jiang, “Lead: Learning decomposition for source-free universal domain adaptation,” in *The IEEE/CVF Conference on Computer Vision and Pattern Recognition*, 2024, pp. 23 334–23 343.
- [27] Y. Wang, K. Zhang, M. Wang, S. Gao, and N. Yin, “Usbd: Universal structural basis distillation for source-free graph domain adaptation,” *arXiv preprint arXiv:2602.08431*, 2026.
- [28] U. Hwang, J. Lee, J. Shin, and S. Yoon, “Sf(da)²: Source-free domain adaptation through the lens of data augmentation,” *arXiv preprint arXiv:2403.10834*, 2024.
- [29] H. Xia, H. Zhao, and Z. Ding, “Adaptive adversarial network for source-free domain adaptation,” in *The IEEE/CVF Conference on Computer Vision and Pattern Recognition*, 2021, pp. 9010–9019.
- [30] S. Roy, M. Trapp, A. Pilzer, J. Kannala, N. Sebe, E. Ricci, and A. Solin, “Uncertainty-guided source-free domain adaptation,” in *European conference on computer vision*. Springer, 2022, pp. 537–555.
- [31] X. Yu, Z. Gong, C. Zhou, Y. Fang, and H. Zhang, “Samgpt: Text-free graph foundation model for multi-domain pre-training and cross-domain adaptation,” in *Proceedings of the ACM Web Conference*, 2025, pp. 1142–1153.
- [32] Z. Zhang and B. He, “Aggregate to adapt: Node-centric aggregation for multi-source-free graph domain adaptation,” in *Proceedings of the ACM Web Conference*, 2025, pp. 4420–4431.
- [33] J. Luo, H. Tao, X. Luo, Y. Zhao, Z. Xiao, D. He, W. Ju, C. Chen, X.-S. Hua, and M. Zhang, “Robust cross supervision with target mining for source-free graph domain adaptation,” *IEEE Transactions on Knowledge and Data Engineering*, 2026.
- [34] Y. Luo, Z. Wang, Z. Chen, Z. Huang, and M. Bakhtashmotlagh, “Source-free progressive graph learning for open-set domain adaptation,” *IEEE Transactions on Pattern Analysis and Machine Intelligence*, vol. 45, no. 9, pp. 11 240–11 255, 2023.
- [35] Z. Zeng, J. Xie, Z. Yang, T. Ma, and D. Chen, “To-ugda: target-oriented unsupervised graph domain adaptation,” *Scientific Reports*, vol. 14, no. 1, p. 9165, 2024.
- [36] W. Chen, G. Ye, Y. Wang, Z. Zhang, L. Zhang, D. Wang, Z. Zhang, and F. Zhuang, “Smoothness really matters: A simple yet effective approach for unsupervised graph domain adaptation,” in *Proceedings of the AAAI Conference on Artificial Intelligence*, vol. 39, no. 15, 2025, pp. 15 875–15 883.
- [37] S. Yang, S. Wu, E. Yang, B. Han, Y. Liu, M. Xu, G. Niu, and T. Liu, “A parametrical model for instance-dependent label noise,” *IEEE Transactions on Pattern Analysis and Machine Intelligence*, vol. 45, no. 12, pp. 14 055–14 068, 2023.
- [38] Y. Zhu, L. Feng, Z. Deng, Y. Chen, R. Amor, and M. Witbrock, “Robust node classification on graph data with graph and label noise,” in *Proceedings of the AAAI Conference on Artificial Intelligence*, vol. 38, 2024, pp. 17 220–17 227.
- [39] H. Song, M. Kim, D. Park, Y. Shin, and J.-G. Lee, “Learning from noisy labels with deep neural networks: A survey,” *IEEE transactions on neural networks and*

- learning systems*, vol. 34, no. 11, pp. 8135–8153, 2022.
- [40] B. Han, Q. Yao, T. Liu, G. Niu, I. W. Tsang, J. T. Kwok, and M. Sugiyama, “A survey of label-noise representation learning: Past, present and future,” *arXiv preprint arXiv:2011.04406*, 2020.
- [41] N. Yin, L. Shen, C. Chen, X.-S. Hua, and X. Luo, “Sport: A subgraph perspective on graph classification with label noise,” *ACM Transactions on Knowledge Discovery from Data*, vol. 18, no. 9, pp. 1–20, 2024.
- [42] D. Angluin and P. Laird, “Learning from noisy examples,” *Machine learning*, vol. 2, no. 4, pp. 343–370, 1988.
- [43] N. Natarajan, I. S. Dhillon, P. K. Ravikumar, and A. Tewari, “Learning with noisy labels,” *Advances in neural information processing systems*, vol. 26, 2013.
- [44] Y. LeCun, L. Bottou, Y. Bengio, and P. Haffner, “Gradient-based learning applied to document recognition,” *Proceedings of the IEEE*, 2002.
- [45] A. Krizhevsky, G. Hinton *et al.*, “Learning multiple layers of features from tiny images,” 2009.
- [46] N. Yin, L. Shen, M. Wang, X. Liu, C. Chen, and X.-S. Hua, “Dream: a dual variational framework for unsupervised graph domain adaptation,” *IEEE Transactions on Pattern Analysis and Machine Intelligence*, 2025.
- [47] N. Shervashidze, P. Schweitzer, E. J. Van Leeuwen, K. Mehlhorn, and K. M. Borgwardt, “Weisfeiler-lehman graph kernels.” *Journal of Machine Learning Research*, vol. 12, no. 9, 2011.
- [48] T. N. Kipf and M. Welling, “Semi-supervised classification with graph convolutional networks,” in *Proceedings of the International Conference on Machine Learning*, 2017.
- [49] K. Xu, W. Hu, J. Leskovec, and S. Jegelka, “How powerful are graph neural networks?” in *Proceedings of the International Conference on Machine Learning*, 2018.
- [50] C. Bodnar, F. Frasca, N. Otter, Y. Wang, P. Lio, G. F. Montufar, and M. Bronstein, “Weisfeiler and lehman go cellular: Cw networks,” *Proceedings of the Conference on Neural Information Processing Systems*, vol. 34, pp. 2625–2640, 2021.
- [51] J. Baek, M. Kang, and S. J. Hwang, “Accurate learning of graph representations with graph multiset pooling,” *arXiv preprint arXiv:2102.11533*, 2021.
- [52] G. Michel, G. Nikolentzos, J. F. Lutzeyer, and M. Vazirgiannis, “Path neural networks: Expressive and accurate graph neural networks,” in *Proceedings of the International Conference on Machine Learning*. PMLR, 2023, pp. 24 737–24 755.
- [53] G. Xu, H. Guo, L. Yi, C. Ling, B. Wang, and G. Yi, “Revisiting source-free domain adaptation: a new perspective via uncertainty control,” in *Proceedings of the International Conference on Learning Representations*, vol. 2025, 2025, pp. 92 900–92 939.
- [54] Z. Zhang, M. Liu, A. Wang, H. Chen, Z. Li, J. Bu, and B. He, “Collaborate to adapt: Source-free graph domain adaptation via bi-directional adaptation,” in *Proceedings of the ACM Web Conference*, 2024, pp. 664–675.
- [55] N. Yin, L. Shen, B. Li, M. Wang, X. Luo, C. Chen, Z. Luo, and X.-S. Hua, “Deal: An unsupervised domain adaptive framework for graph-level classification,” in *Proceedings of the ACM International Conference on Multimedia*, 2022, pp. 3470–3479.
- [56] P. D. Dobson and A. J. Doig, “Distinguishing enzyme structures from non-enzymes without alignments,” *Journal of molecular biology*, vol. 330, no. 4, pp. 771–783, 2003.
- [57] N. Wale, I. A. Watson, and G. Karypis, “Comparison of descriptor spaces for chemical compound retrieval and classification,” *Knowledge and Information Systems*, vol. 14, pp. 347–375, 2008.
- [58] J. Kazius, R. McGuire, and R. Bursi, “Derivation and validation of toxicophores for mutagenicity prediction,” *Journal of medicinal chemistry*, vol. 48, no. 1, pp. 312–320, 2005.
- [59] F. Orsini, P. Frasconi, and L. De Raedt, “Graph invariant kernels,” in *Proceedings of the International Joint Conference on Artificial Intelligence*, 2015.
- [60] W. Hu, M. Fey, H. Ren, M. Nakata, Y. Dong, and J. Leskovec, “Ogb-lsc: A large-scale challenge for machine learning on graphs,” *arXiv preprint arXiv:2103.09430*, 2021.
- [61] V. P. Dwivedi, C. K. Joshi, A. T. Luu, T. Laurent, Y. Bengio, and X. Bresson, “Benchmarking graph neural networks,” *The Journal of Machine Learning Research.*, 2023.

APPENDIX

This appendix provides detailed proofs, implementation details, and additional experimental protocols for S²PLR. The notation follows Sections III-E–IV. The purpose of the appendix is to make explicit the distinction between two notions that are easy to conflate: (i) a population noise bound on selected pseudo labels and (ii) target-only structural certificates used to identify reliable samples in practice.

A. Detailed Proofs

1) *Proof of Theorem 2:* Let $x \in \mathcal{H}_{\tau, \rho}$ and denote its pseudo-label by $c = \tilde{y}(x)$. By the definition of the safe subspace in Eq. (1), we have

$$p_S(c | x) = s(x) \geq \tau. \quad (21)$$

Assumption 1 then gives

$$p_T(c | x) \geq p_S(c | x) - \beta_\tau(\alpha) \geq \tau - \beta_\tau(\alpha). \quad (22)$$

Since $\eta(x) = \Pr[\tilde{y}(x) \neq y | x] = 1 - p_T(c | x)$, we obtain

$$\eta(x) \leq 1 - \tau + \beta_\tau(\alpha), \quad (23)$$

which proves Eq. (2).

We next prove the aggregate neighborhood certificate. For any $x' \in \mathcal{N}_{\text{same}}^\tau(x)$, the construction of $\mathcal{N}_{\text{same}}^\tau(x)$ implies $\tilde{y}(x') = \tilde{y}(x) = c$ and $s(x') \geq \tau$. Applying Assumption 1 at x' yields

$$p_T(c | x') \geq p_S(c | x') - \beta_\tau(\alpha) \geq \tau - \beta_\tau(\alpha). \quad (24)$$

Moreover, because $x \in \mathcal{H}_{\tau, \rho}$, at least a ρ -fraction of the target neighborhood $\mathcal{N}(x)$ belongs to $\mathcal{N}_{\text{same}}^\tau(x)$. The posterior probabilities of the remaining neighbors are nonnegative. Therefore,

$$\frac{1}{|\mathcal{N}(x)|} \sum_{x' \in \mathcal{N}(x)} p_T(c | x') \geq \frac{|\mathcal{N}_{\text{same}}^\tau(x)|}{|\mathcal{N}(x)|} (\tau - \beta_\tau(\alpha)) \quad (25)$$

$$\geq \rho(\tau - \beta_\tau(\alpha)), \quad (26)$$

which proves Eq. (3).

Finally, we prove the geometric certificate. For any $x' \in \mathcal{N}_{\text{same}}^\tau(x)$, Assumption 2 gives

$$p_T(c | x) \geq p_T(c | x') - Ld(x, x'). \quad (27)$$

Combining this inequality with the lower bound on $p_T(c | x')$ gives

$$p_T(c | x) \geq \tau - \beta_\tau(\alpha) - Ld(x, x'). \quad (28)$$

Averaging over $x' \in \mathcal{N}_{\text{same}}^\tau(x)$ yields

$$p_T(c | x) \geq \tau - \beta_\tau(\alpha) - L \frac{1}{|\mathcal{N}_{\text{same}}^\tau(x)|} \sum_{x' \in \mathcal{N}_{\text{same}}^\tau(x)} d(x, x'), \quad (29)$$

which is Eq. (4). If $\tau - \beta_\tau(\alpha) > 1/2$, then Eq. (2) implies $\eta(x) < 1/2$ for every $x \in \mathcal{H}_{\tau, \rho}$, which is the Massart bounded-noise condition on the selected safe subspace.

a) *Remark on the role of ρ :* The proof intentionally separates the pointwise noise bound from the structural certificates. Under Assumption 1, the pointwise pseudo-label noise at the center sample is already controlled by τ and $\beta_\tau(\alpha)$. The neighborhood ratio ρ should not be interpreted as a factor that directly multiplies the center-point posterior. Instead, ρ provides observable target-domain evidence that the selected pseudo-label is locally supported rather than an isolated high-confidence error. This is why ρ enters the empirical safe-subspace selection rule in Eq. (16), while the Massart noise condition follows from Eq. (2).

2) *Proof of Proposition 1:* For a fixed target representation x , define the Bernoulli variable

$$B_i = \mathbb{I}[\tilde{y}(x_i) = \tilde{y}(x), s(x_i) \geq \tau], \quad (30)$$

where x_i is the i -th sampled neighbor of x . The empirical structural gate is

$$\hat{r}_\tau(x) = \frac{1}{k_{\text{nn}}} \sum_{i=1}^{k_{\text{nn}}} B_i, \quad (31)$$

and its population counterpart is $r_\tau(x) = \mathbb{E}[B_i]$. Hoeffding's inequality gives

$$\Pr[|\hat{r}_\tau(x) - r_\tau(x)| \geq \epsilon] \leq 2 \exp(-2k_{\text{nn}}\epsilon^2). \quad (32)$$

Setting the right-hand side to δ proves Eq. (5). If $\hat{r}_\tau(x) \geq \rho_{\min} + \epsilon$, then with the same probability,

$$r_\tau(x) \geq \hat{r}_\tau(x) - \epsilon \geq \rho_{\min}. \quad (33)$$

This proves the finite-sample reliability statement.

3) *Proof of Corollary 2:* Fix $x \in \mathcal{H}_{\tau, \rho}$. Let $Z_k = \mathbb{I}[f_S^k(x) \neq y]$ be the error indicator of the k -th source expert. Under the idealized condition in Corollary 2, the variables Z_1, \dots, Z_{K_e} are conditionally independent given x , and $\mathbb{E}[Z_k | x] \leq \bar{e} < 1/2$. Majority voting is wrong only when

$$\frac{1}{K_e} \sum_{k=1}^{K_e} Z_k \geq \frac{1}{2}. \quad (34)$$

Hoeffding's inequality gives

$$\Pr\left[\frac{1}{K_e} \sum_{k=1}^{K_e} Z_k \geq \frac{1}{2} \mid x\right] \leq \Pr\left[\frac{1}{K_e} \sum_{k=1}^{K_e} Z_k - \bar{e} \geq \frac{1}{2} - \bar{e} \mid x\right] \quad (35)$$

$$\leq \exp\left(-2K_e \left(\frac{1}{2} - \bar{e}\right)^2\right). \quad (36)$$

This proves Eq. (7).

The conditional-independence assumption is only a sufficient condition for the closed-form exponential bound. In practice, source checkpoints trained on the same source domain can have correlated errors. For this reason, S²PLR does not use Eq. (7) as an unconditional performance guarantee. Instead, it uses the committee to measure empirical consensus and predictive variance through Eqs. (10)–(11). A target graph is admitted into \mathcal{S}_{sem} only when the committee is both confident and low-disagreement, and it must further pass the structural gate in Eq. (16) before hard pseudo-label supervision is used.

4) *Proof of Proposition 2:* Let $\mathcal{U} = \mathcal{X}_T \setminus \mathcal{H}_{\tau, \rho}$. The target risk can be decomposed as

$$R_T(h) = \Pr[h(x) \neq y, x \in \mathcal{H}_{\tau, \rho}] + \Pr[h(x) \neq y, x \in \mathcal{U}] \quad (37)$$

$$= \pi_{\mathcal{H}} \Pr[h(x) \neq y \mid x \in \mathcal{H}_{\tau, \rho}] + \pi_{\mathcal{U}} R_{\mathcal{U}}(h). \quad (38)$$

On the safe subspace, the event $h(x) \neq y$ is contained in the union of the two events $h(x) \neq \tilde{y}(x)$ and $\tilde{y}(x) \neq y$. Hence

$$\Pr[h(x) \neq y \mid x \in \mathcal{H}_{\tau, \rho}] \leq \Pr[h(x) \neq \tilde{y}(x) \mid x \in \mathcal{H}_{\tau, \rho}] + \Pr[\tilde{y}(x) \neq y \mid x \in \mathcal{H}_{\tau, \rho}] \quad (39)$$

$$\leq \tilde{R}_{\mathcal{H}}(h) + \bar{\eta}_\tau. \quad (40)$$

Substituting this inequality into the risk decomposition gives Eq. (8). If the uncertain-set risk is upper bounded by a regularizer-induced quantity $R_{\mathcal{U}}(h) \leq \Gamma_{\mathcal{U}}(h)$, then replacing $R_{\mathcal{U}}(h)$ with $\Gamma_{\mathcal{U}}(h)$ gives Eq. (9).

5) *A finite-sample variant:* The previous proposition is a population decomposition. For completeness, we state a standard finite-sample form that explains the empirical objective in Eq. (20). Suppose m selected target graphs are sampled from $\mathcal{H}_{\tau, \rho}$, and let $\tilde{R}_{\mathcal{H}}(h)$ be the empirical pseudo-label risk on them. For a bounded classification loss and a hypothesis class with Rademacher complexity $\mathfrak{R}_m(\mathcal{H})$, with probability at least $1 - \delta$, uniformly over h ,

$$\tilde{R}_{\mathcal{H}}(h) \leq \hat{R}_{\mathcal{H}}(h) + 2\mathfrak{R}_m(\mathcal{H}) + \sqrt{\frac{\log(2/\delta)}{2m}}. \quad (41)$$

Combining this inequality with Proposition 2 gives

$$R_T(h) \leq \pi_{\mathcal{H}} \left(\hat{R}_{\mathcal{H}}(h) + \bar{\eta}_\tau + 2\mathfrak{R}_m(\mathcal{H}) + \sqrt{\frac{\log(2/\delta)}{2m}} \right) + \pi_{\mathcal{U}} \Gamma_{\mathcal{U}}(h). \quad (42)$$

This finite-sample variant should be read as a conventional generalization statement for the selected pseudo-labeled subset. It is not used to claim that pseudo-labels are reliable on the full target domain.

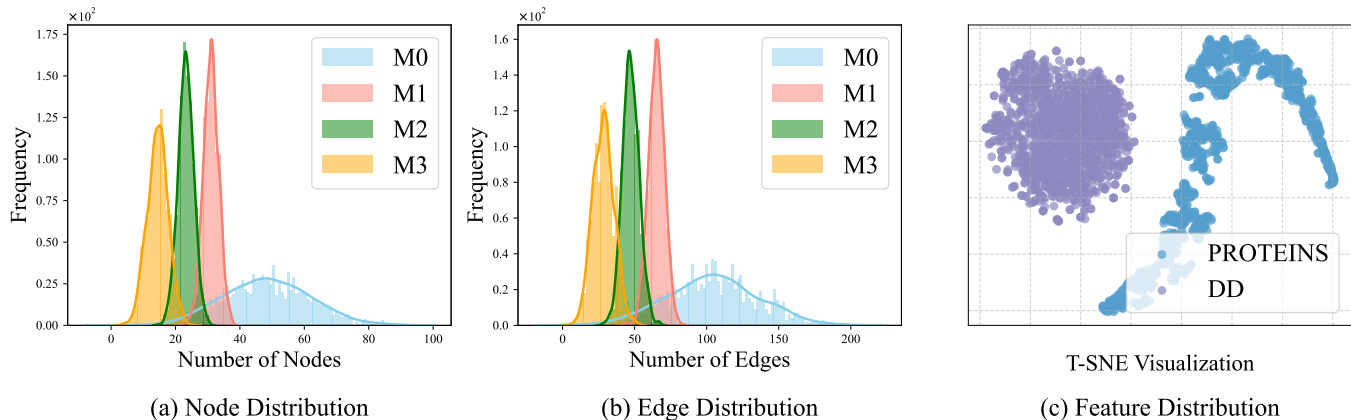


Fig. 4: Visualization of domain shifts across different types. (a,b) Node and edge distribution shifts between sub-datasets of Mutagenicity. (c) Feature distribution shift between PROTEINS and DD datasets.

TABLE VIII: Statistics of the experimental datasets.

Datasets	Graphs	Avg. Nodes	Avg. Edges	Classes
DD	1,178	284.32	715.66	2
NCI1	4,110	29.87	32.30	2
Mutagenicity	4,337	30.32	30.77	2
FRANKENSTEIN	4,337	16.9	17.88	2
ogbg-molhiv	41,127	25.5	27.5	2
CIFAR10	60,000	117.6	941.2	10
MNIST	70,000	70.6	564.5	10
PROTEINS	1,113	39.1	72.8	2
COX2	467	41.22	43.45	2
COX2_MD	303	26.28	335.12	2
BZR	405	35.75	38.36	2
BZR_MD	306	21.30	225.06	2

B. Connection to Full-Domain Unbounded-Noise Analyses

The safe-subspace guarantee does not contradict the full-domain unbounded-noise result in Theorem 1. The two statements analyze different adaptation protocols. The unbounded-noise result shows that if a fixed source classifier is applied to all shifted target samples, then there may exist a target region on which pseudo-labels are almost surely wrong. Our analysis instead studies a selective protocol in which hard pseudo-label supervision is restricted to

$$\mathcal{H}_{\tau,\rho} = \{x : s(x) \geq \tau, r_{\tau}(x) \geq \rho\}. \quad (43)$$

Samples outside this set are not discarded; they are used through soft target regularization. Therefore, the theory should be interpreted as a sufficient condition for reliable selective adaptation, not as a global claim that every source-free pseudo-label is bounded-noise.

This distinction also explains the design of S²PLR. Module I estimates semantic reliability through source confidence and ensemble disagreement. Module II learns a target-intrinsic representation in which neighborhood evidence is more meaningful. Module III intersects semantic and structural evidence to form $\mathcal{H}_{\zeta,\rho}$. Module IV avoids assigning hard labels to the remaining uncertain samples and instead controls them through entropy and KL regularization.

C. Dataset

1) *Dataset Description*: We provide additional details of the datasets used in our experiments. For structure-based domain shifts, we use real-world graph benchmarks and image-derived graph benchmarks. For graph datasets, molecules are represented as graphs with atoms as nodes and chemical bonds as edges, while proteins are represented with amino acids as nodes and spatial or chemical proximity relations as edges. Following [8, 46, 55], we construct structural domains by sorting graphs according to graph-level structural statistics. Specifically, node-density shifts are generated by sorting graphs according to the number of nodes $|V|$, while edge-density shifts are generated by sorting graphs according to the number of edges $|E|$. The sorted graphs are then divided into quantile-based subdomains with a shared label space.

(1) Structure-based domain shifts.

TABLE IX: Subdomain statistics for density-based partitions. *Avg. Struct.* and *Std. Struct.* denote the mean and standard deviation of the corresponding structural metrics. Class 0 and Class 1 are reported only for binary datasets; class counts for MNIST and CIFAR10 are omitted because they contain 10 classes.

Dataset	Split	Domain	#Graphs	Class 0	Class 1	Avg. Struct.	Std. Struct.
Mutagenicity	Node	M0	1084	515	569	52.71	28.12
Mutagenicity	Node	M1	1084	730	354	31.00	2.37
Mutagenicity	Node	M2	1084	649	435	23.16	2.42
Mutagenicity	Node	M3	1085	507	578	14.41	3.32
Mutagenicity	Edge	M0	1084	557	527	52.80	16.91
Mutagenicity	Edge	M1	1084	723	361	32.55	2.70
Mutagenicity	Edge	M2	1084	618	466	23.66	2.81
Mutagenicity	Edge	M3	1085	503	582	14.08	3.64
NCII	Node	N0	1027	277	750	47.97	13.78
NCII	Node	N1	1027	504	523	30.59	2.43
NCII	Node	N2	1027	588	439	23.83	1.72
NCII	Node	N3	1029	684	345	17.09	3.03
NCII	Edge	N0	1027	281	746	52.25	14.98
NCII	Edge	N1	1027	524	503	33.16	2.67
NCII	Edge	N2	1027	546	481	25.79	1.86
NCII	Edge	N3	1029	702	327	18.04	3.54
FRANKENSTEIN	Node	F0	1084	468	616	28.46	14.17
FRANKENSTEIN	Node	F1	1084	355	729	18.13	1.42
FRANKENSTEIN	Node	F2	1084	457	627	13.08	1.47
FRANKENSTEIN	Node	F3	1085	656	429	7.93	2.06
FRANKENSTEIN	Edge	F0	1084	434	650	31.13	14.81
FRANKENSTEIN	Edge	F1	1084	363	721	19.54	1.70
FRANKENSTEIN	Edge	F2	1084	484	600	13.43	1.74
FRANKENSTEIN	Edge	F3	1085	655	430	7.42	2.35
DD	Node	D0	294	54	240	96.69	28.71
DD	Node	D1	295	153	142	191.05	29.01
DD	Node	D2	294	233	61	298.36	32.55
DD	Node	D3	295	251	44	550.58	421.71
DD	Edge	D0	294	57	237	229.79	70.62
DD	Edge	D1	295	153	142	470.15	74.44
DD	Edge	D2	294	227	67	746.97	82.80
DD	Edge	D3	295	254	41	1414.19	1058.74
ogbg-molhiv	Node	H0	10281	10080	201	14.90	2.65
ogbg-molhiv	Node	H1	10281	9972	309	20.74	1.35
ogbg-molhiv	Node	H2	10281	9987	294	25.92	1.85
ogbg-molhiv	Node	H3	10284	9645	639	40.48	14.66
ogbg-molhiv	Edge	H0	10281	10079	202	15.54	3.07
ogbg-molhiv	Edge	H1	10281	9960	321	22.31	1.55
ogbg-molhiv	Edge	H2	10281	9994	287	28.15	2.08
ogbg-molhiv	Edge	H3	10284	9651	633	43.87	15.61
MNIST	Edge	S0	23334	-	-	204.40	20.20
MNIST	Edge	S1	23333	-	-	273.80	26.26
MNIST	Edge	S2	23333	-	-	360.41	33.79
CIFAR10	Edge	C0	20000	-	-	400.52	14.96
CIFAR10	Edge	C1	20000	-	-	593.02	21.92
CIFAR10	Edge	C2	20000	-	-	795.90	29.14

- **DD.** DD [56] contains 1,178 protein graphs for binary classification, where each graph is labeled according to whether the protein is an enzyme. Compared with PROTEINS, DD graphs are typically larger and denser, making the dataset suitable for evaluating structural shifts with higher graph complexity. We partition DD into four subdomains, denoted as D0, D1, D2, and D3.
- **NCII.** NCII [57] consists of 4,110 molecular graphs. Each graph corresponds to a chemical compound, and the prediction task is to determine whether the compound is active against cancer cell growth. We divide NCII into four structure-based subdomains, denoted as N0, N1, N2, and N3.
- **Mutagenicity.** Mutagenicity [58] contains 4,337 molecular graphs labeled by mutagenic effect. The dataset contains diverse molecular sizes and bonding patterns, which naturally induce structural heterogeneity. We split it into four subdomains, denoted as M0, M1, M2, and M3.
- **FRANKENSTEIN.** FRANKENSTEIN [59] includes 4,337 molecular graphs for biological activity prediction. The graphs are relatively small compared with several other molecular benchmarks, providing a complementary setting for evaluating adaptation across different graph-size regimes. We partition the dataset into F0, F1, F2, and F3.
- **ogbg-molhiv.** ogbg-molhiv [60] is an OGB molecular benchmark with 41,127 graphs, where the task is to predict whether a molecule inhibits HIV replication. Compared with the TUDataset benchmarks, it is larger and more class-imbalanced, offering a more realistic molecular adaptation scenario. We construct four structural subdomains, denoted as H0, H1, H2,

and H3.

- **MNIST**. MNIST [44] contains 70,000 grayscale digit images from 10 classes. We convert each image into a graph representation, where nodes correspond to pixels or superpixels and edges encode spatial adjacency. The resulting graphs are partitioned into three edge-based subdomains, denoted as S0, S1, and S2.
- **CIFAR-10**. CIFAR-10 [45] contains 60,000 color images from 10 object categories. Similar to MNIST, each image is transformed into a graph with local image regions as nodes and spatial neighborhood relations as edges. We construct three edge-based subdomains, denoted as C0, C1, and C2.

(2) **Feature-based domain shifts**. For feature-based domain shifts, we evaluate paired domains that share the same prediction semantics but differ in node-feature distributions. These tasks test whether a method can adapt when the global graph-level semantics are comparable but the local feature statistics change across domains.

- **PROTEINS and DD**. PROTEINS [56] contains 1,113 protein graphs for binary graph classification, with labels indicating enzyme or non-enzyme classes. Together with DD, it forms the PROTEINS \leftrightarrow DD transfer pair. This pair evaluates adaptation across protein graph domains with related label semantics but different graph and feature characteristics.
- **COX2 and COX2_MD**. COX2 contains 467 molecular graphs, while COX2_MD contains 303 molecular graphs from a modified domain with the same label space. Both datasets describe molecular structures and are used as the COX2 \leftrightarrow COX2_MD transfer pair. This setting evaluates feature-based distribution shifts between related molecular domains.
- **BZR and BZR_MD**. BZR contains 405 molecular graphs, and BZR_MD contains 306 molecular graphs from the corresponding modified domain. The two datasets share the same binary prediction semantics and form the BZR \leftrightarrow BZR_MD transfer pair. This pair provides another molecular feature-shift benchmark with consistent label space but shifted node-feature statistics.

Table IX provides detailed statistics of the constructed subdomains for all structure-based benchmarks. For each dataset and split type, it reports the subdomain identifier, number of graphs, class distribution, and the mean and standard deviation of the corresponding structural statistic. For node-density splits, Avg. Struct. and Std. Struct. refer to the number of nodes; for edge-density splits, they refer to the number of edges used to characterize graph connectivity. These statistics show that the constructed subdomains exhibit clear differences in graph scale or connectivity while maintaining the same label space, thereby forming meaningful structural domain shifts. They also reveal that density-based partitioning may introduce class-prior variations across subdomains, which makes the source-free adaptation setting more realistic and challenging.

2) *Data Processing*: For real-world graph datasets from TUDataset⁴, including DD, PROTEINS, Mutagenicity, NCI1, FRANKENSTEIN, BZR, BZR_MD, COX2, and COX2_MD, we follow the standard preprocessing pipeline provided by PyTorch Geometric⁵. Each graph is converted into a PyG data object, with the original node attributes or node labels used as input features when available. For image benchmarks, i.e., MNIST and CIFAR10, we transform each image into a graph representation. Nodes correspond to pixels or superpixels, and edges are constructed according to spatial proximity. Specifically, we build KNN graphs based on node spatial coordinates, where the neighborhood size is adjusted to control graph density and induce edge-density domain shifts [9, 61]. The original image category is used as the graph-level label. For datasets from the Open Graph Benchmark (OGB)⁶, such as ogbg-molhiv, we follow the official OGB preprocessing and evaluation protocol. The molecular graphs are loaded with their provided atom and bond features, and the ROC-AUC metric is used following the standard OGB setting.

D. Baselines

We compare the proposed S²PLR with a comprehensive set of competitive baselines on the datasets above. These baselines include six graph kernels and general graph neural networks, including WL [47], PathNN [52], GCN [48], GIN [49], CIN [50], and GMT [51]; four source-free domain adaptation methods: SFDA_LLN [19], SF(DA)² [28], NVC_LLN [20], and Ucon_SFDA [53]; four source-free graph domain adaptation methods: SOGA [15], GraphCTA [54], GALA [16], and GraphATA [32].

- **WL**: The Weisfeiler–Lehman (WL) graph kernel [47] captures hierarchical graph structures by iteratively relabeling nodes based on neighborhood information. It computes graph similarities through subtree pattern matching, enabling efficient and expressive structural comparison.
- **PathNN**: Path Neural Networks (PathNN) [52] enhance the expressive power of graph neural networks by modeling relationships along paths rather than only adjacent nodes. They aggregate path-based representations through attention mechanisms, effectively capturing higher-order structural dependencies and improving graph-level prediction accuracy.
- **GCN**: Graph Convolutional Networks (GCN) [48] perform graph learning by propagating and aggregating feature information from neighboring nodes through spectral convolutions. This approach effectively captures local graph structure while enabling efficient end-to-end training.

⁴<https://chrsmrrs.github.io/datasets/>

⁵<https://pyg.org/>

⁶<https://ogb.stanford.edu/>

TABLE X: Paired Wilcoxon signed-rank tests on reported task-level mean performance over all node- and edge-shift transfer tasks, with Holm correction for multiple comparisons.

Comparison	Test Scope	Test Statistic W	Holm-adjusted p -value	Significant at 0.05
S ² PLR vs. GraphATA	132 node/edge tasks	849.0	8.94×10^{-16}	Yes
S ² PLR vs. GALA	132 node/edge tasks	810.0	8.65×10^{-16}	Yes
S ² PLR vs. GraphCTA	132 node/edge tasks	521.5	7.43×10^{-18}	Yes
S ² PLR vs. SOGA	132 node/edge tasks	378.0	3.29×10^{-19}	Yes
S ² PLR vs. UCon_SFDA	132 node/edge tasks	272.5	4.39×10^{-20}	Yes
S ² PLR vs. NVC_LLN	132 node/edge tasks	73.5	8.84×10^{-22}	Yes
S ² PLR vs. SF(DA) ²	132 node/edge tasks	137.5	4.14×10^{-21}	Yes
S ² PLR vs. SFDA_LLN	132 node/edge tasks	103.0	1.50×10^{-21}	Yes

- **GIN**: Graph Isomorphism Networks (GIN) [49] achieve maximal discriminative power among message-passing GNNs by using sum aggregation and multi-layer perceptrons to capture injective neighborhood functions, enabling them to distinguish complex graph structures equivalent to the Weisfeiler–Lehman test.
- **CIN**: Cellular Weisfeiler–Lehman Networks (CIN) [50] extend the Weisfeiler–Lehman framework to higher-dimensional cellular complexes, enabling message passing beyond edges to higher-order cells. This design captures multi-scale structural interactions and richer topological dependencies in complex graphs.
- **GMT**: Graph Multiset Transformer (GMT) [51] introduces attention-based multiset pooling to learn expressive graph-level representations. By employing learnable queries to aggregate node embeddings, GMT flexibly captures diverse structural patterns and global dependencies for accurate graph representation learning.
- **SFDA_LLN**: SFDA_LLN [19] introduces a robust source-free domain adaptation framework that models label noise as unbounded and exploits the early-time training phenomenon (ETP) to prevent noise memorization. By incorporating early-learning regularization into the SFDA objective, it effectively mitigates noisy pseudo-labels and significantly improves cross-domain adaptation performance.
- **SF(DA)²**: SF(DA)² [28] reinterprets source-free domain adaptation from a data augmentation perspective. It generates diverse target-domain variants to simulate source data, enabling model adaptation through consistency regularization and self-training without requiring access to source samples.
- **NVC_LLN**: NVC_LLN [20] provides a theoretical and empirical analysis of label noise in SFDA, distinguishing between bounded and unbounded noise regimes. It introduces principled strategies to mitigate noise-induced degradation, offering both theoretical insights and practical algorithms that enhance adaptation robustness across domains.
- **Ucon_SFDA**: Ucon_SFDA [53] revisits source-free domain adaptation from the perspective of uncertainty control. It explicitly models and regulates target-side uncertainty to reduce unreliable pseudo-labeling, thereby improving adaptation robustness without accessing source data.
- **SOGA**: SOGA [15] introduces a graph-based framework for source-free domain adaptation. It transfers knowledge from a pre-trained source model to the target domain by aligning graph structural features and node representations without accessing source data, leveraging graph topology to enhance domain-invariant learning and cross-domain generalization.
- **GraphCTA**: GraphCTA [54] proposes source-free graph domain adaptation via bi-directional collaboration between source hypothesis and target structure, iteratively refining pseudo-labels and representations through consistency, topology-aware alignment, and cooperative training to improve cross-domain generalization.
- **GALA**: GALA [16] introduces a diffusion-driven graph alignment framework that preserves structural consistency between domains. It employs a jigsaw-style self-supervised task to enhance feature discrimination and jointly optimizes diffusion alignment and representation learning, enabling robust adaptation without access to source data.
- **GraphATA**: GraphATA [32] addresses multi-source-free graph domain adaptation through node-centric aggregation. It dynamically aggregates knowledge from multiple source hypotheses according to local graph context, enabling fine-grained target adaptation without using source graphs.

All methods are evaluated on the same source-target splits. Results are reported as mean performance with standard deviation over five random seeds. Small numerical differences whose standard-deviation ranges overlap are treated as empirically comparable rather than as strict wins. This convention is important because several transfer pairs have margins that are smaller than the run-to-run variance.

E. Algorithm

The complete training procedure is summarized in Algorithm 1.

F. More experimental results

1) *More performance comparison*: In this section, we present additional performance comparisons between S²PLR and all baseline methods on more graph benchmarks, as summarized in Tables XVI–XXV. The results cover node-density and

Algorithm 1 Training Procedure of S²PLR

```

1: Input: Source experts  $\mathcal{M}$ , target data  $\mathcal{D}^t$ , thresholds  $\zeta, \rho_{\min}$ , variance percentile  $q_u$ , neighborhood size  $k_{\text{nn}}$ , maximum epochs  $E_{\text{max}}$ .
2: Output: Adapted target model  $f_T$ .
3: Initialize  $f_T$  from the primary source checkpoint and initialize the target structure encoder  $g_\psi$ .
4: Warm up  $g_\psi$  on target graphs by minimizing  $\mathcal{L}_{\text{GCL}}$  in Eq. (14).
5: for epoch = 1 to  $E_{\text{max}}$  do
6:   Compute ensemble consensus  $\bar{p}_j$ , pseudo-label  $\hat{y}_j$ , confidence  $s_j$ , and variance  $u_j$  for all  $G_j^t \in \mathcal{D}^t$ .
7:   Set  $\nu = Q_{q_u}(\{u_j\}_{j=1}^{n_t})$ .
8:   Select semantic candidates  $\mathcal{S}_{\text{sem}}$  using Eq. (12).
9:   Compute target structural embeddings with  $g_\psi$  and construct the  $k_{\text{nn}}$ -nearest-neighbor graph.
10:  Compute  $\rho_j$  using Eq. (15) and identify  $\mathcal{H}_{\zeta, \rho}$  using Eq. (16).
11:  Set  $\mathcal{U} = \mathcal{D}^t \setminus \mathcal{H}_{\zeta, \rho}$ .
12:  for each mini-batch  $\mathcal{B} \subset \mathcal{D}^t$  do
13:    Compute  $\mathcal{L}_{\mathcal{H}}$  on  $\mathcal{B} \cap \mathcal{H}_{\zeta, \rho}$  using Eq. (19).
14:    Compute  $\mathcal{L}_{\text{reg}}$  on  $\mathcal{B} \cap \mathcal{U}$  using Eq. (18).
15:    Compute  $\mathcal{L}_{\text{GCL}}$  on  $\mathcal{B}$  using Eq. (14).
16:    Update  $f_T$  and  $g_\psi$  by minimizing Eq. (20).
17:  end for
18: end for
19: return  $f_T$ .

```

edge-density domain shifts on DD, FRANKENSTEIN, Mutagenicity, NCI1, and ogbg-molhiv. Overall, S²PLR achieves the best or consistently competitive performance in most transfer settings, further demonstrating its robustness across molecular and protein graph domains.

Compared with conventional graph classifiers and kernel-based methods, S²PLR shows clear advantages because it explicitly addresses source-target structural mismatch during adaptation. Although existing source-free and graph adaptation baselines improve over non-adaptive models, their performance still varies across transfer directions, especially under large graph-size or connectivity shifts. The paired Wilcoxon signed-rank tests in Table X further support this observation. Based on the reported task-level mean performance over 132 node- and edge-shift transfer tasks, S²PLR achieves statistically significant improvements over representative source-free and graph adaptation baselines after Holm correction, including GraphATA, GALA, GraphCTA, SOGA, Ucon_SFDA, NVC_LLN, SF(DA)², and SFDA_LLN. This indicates that the gains of S²PLR are not concentrated on a few favorable transfer pairs, but are consistent across a broad range of structural domain shifts. In particular, the significant improvements over strong graph-specific baselines such as GraphATA, GALA, and GraphCTA suggest that topology-aware adaptation alone is not sufficient; reliable source-free graph adaptation also benefits from multi-expert semantic reliability estimation, target-intrinsic structure learning, neighborhood-consistency verification, and soft regularization on uncertain samples. These results reinforce the conclusion that effective source-free graph adaptation requires both conservative safe-subspace supervision and principled exploitation of the remaining uncertain target data.

2) *More Ablation study:* To further validate the effectiveness of each component in S²PLR, we conduct additional ablation studies on the DD, NCI1, FRANKENSTEIN, and ogbg-molhiv datasets. Specifically, we evaluate five ablated variants of S²PLR, including S²PLR w/o ME, S²PLR w/o CF, S²PLR w/o TS, S²PLR w/o NC, and S²PLR w/o SR. The corresponding experimental results are reported in Tables XII, XIV, XIII, and XV. Overall, the observed trends are consistent with those discussed in Section V-F, further confirming that each component contributes to the robustness of S²PLR under source-free graph domain adaptation.

These ablations also correspond to the theoretical risk decomposition in Proposition 2. Removing multi-expert uncertainty quantification weakens the identification of consensus pseudo-labels and makes the safe set more vulnerable to source-biased predictions. Removing the confidence filter primarily weakens the control of the pseudo-label noise term $\bar{\eta}_\tau$, while removing the neighborhood-consistency gate weakens the empirical certification of the safe subspace $\mathcal{H}_{\tau, \rho}$. Removing the target-intrinsic structure branch makes neighborhood construction less reliable and may enlarge the effective radius term $L\bar{r}$. Removing the soft regularization on the uncertain set \mathcal{U} weakens the control of the uncertain-set risk term $\Gamma_{\mathcal{U}}(h)$. Beyond accuracy, safe-subspace coverage and selected pseudo-label precision are direct post-hoc diagnostics for the selective-learning mechanism. When target labels are used for such analysis, these diagnostics are reported separately from model selection and do not affect the source-free adaptation protocol.

3) *More Sensitivity Analysis:* We further analyze the sensitivity of S²PLR to the confidence threshold ζ and the neighborhood-consistency threshold ρ_{\min} on DD, FRANKENSTEIN, NCI1, and ogbg-molhiv. The results are shown in Fig. 5 and 6, and the observed trends are consistent with the analysis in Section V-G. For each dataset, we vary one threshold at a time over

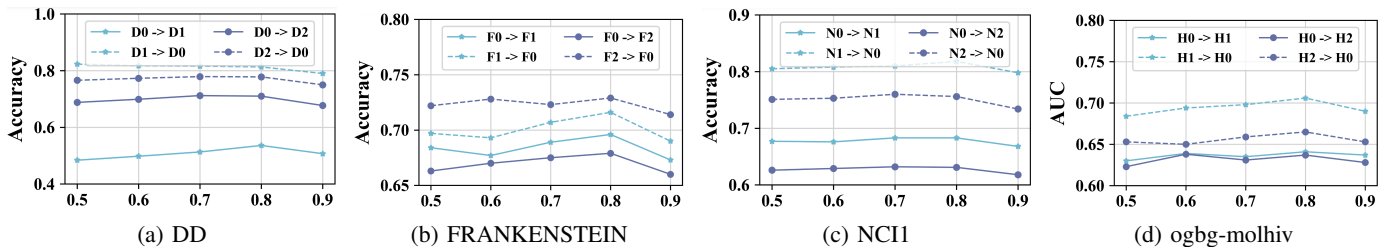


Fig. 5: Sensitivity analysis of the confidence threshold ζ on DD, FRANKENSTEIN, NCI1, and ogbg-molhiv.

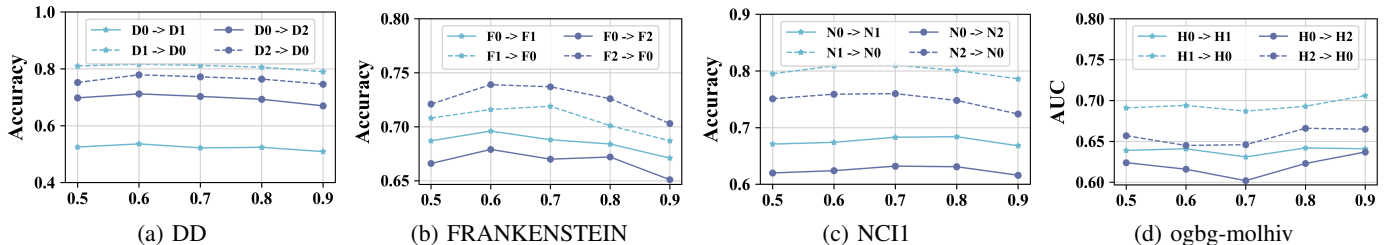


Fig. 6: Sensitivity analysis of the neighborhood-consistency threshold ρ_{\min} on DD, FRANKENSTEIN, NCI1, and ogbg-molhiv.

$\{0.5, 0.6, 0.7, 0.8, 0.9\}$ while keeping the other hyperparameters fixed.

Overall, S^2 PLR exhibits stable performance across a broad range of threshold values. For the confidence threshold ζ , moderate values generally lead to better results because they remove low-confidence pseudo-labels while retaining sufficient safe samples for hard supervision. When ζ becomes too large, the selected safe subspace may become overly conservative, which slightly degrades performance on several transfer directions. For the neighborhood-consistency threshold ρ_{\min} , a similar quality–coverage trade-off can be observed: small values may admit locally inconsistent samples, whereas overly strict values may discard useful target samples under domain shift. Across DD, FRANKENSTEIN, NCI1, and ogbg-molhiv, the best or near-best performance is usually achieved in the middle range, especially around 0.6–0.8. These results confirm that S^2 PLR is not overly sensitive to the exact threshold choice and that its semantic and structural filters remain effective across both molecular and protein graph benchmarks.

We additionally examine the sensitivity of S^2 PLR to the number of source experts K_e , as shown in Fig. 7. We vary K_e from 1 to 6 while keeping the other hyperparameters fixed. The source experts are added cumulatively in the following order: GMT, GIN, PathNN, GCN, SAGE, and RandomWalkNN. Thus, $K_e = 1$ uses only GMT, $K_e = 2$ uses GMT and GIN, $K_e = 3$ uses GMT, GIN, and PathNN, and larger values further include GCN, SAGE, and RandomWalkNN. Different from ζ and ρ_{\min} , which control the strictness of sample selection, K_e affects the reliability of multi-expert uncertainty estimation.

The results show that increasing K_e from a single source hypothesis to a moderate-size heterogeneous committee generally improves performance, indicating that complementary experts provide more stable disagreement signals and help suppress source-biased pseudo-labels. However, the gains tend to saturate when K_e becomes larger, and further increasing the number of experts does not consistently improve performance across datasets. This suggests that additional experts may introduce redundant or less informative disagreement signals, making safe-subspace selection overly conservative in some transfer directions. Overall, the results support the default choice of $K_e = 3$, which uses GMT, GIN, and PathNN and achieves a favorable trade-off between reliability estimation, adaptation performance, and computational cost across Mutagenicity, DD, FRANKENSTEIN, NCI1, and ogbg-molhiv.

4) *Efficiency and Resource Consumption Analysis*: In this section, we report the computational cost of S^2 PLR and representative baselines, including GALA, GraphCTA, and SOGA, in Table XI. The goal is to examine whether the performance gains of S^2 PLR come from a substantially larger adaptation budget or from the proposed reliability-guided refinement mechanism. All measurements are conducted on the Mutagenicity dataset under the same hardware setting. We report the per-epoch adaptation time, peak GPU memory, number of released source hypotheses, and trainable parameters during target adaptation. For S^2 PLR, S^2 PLR-Single uses one frozen GMT source hypothesis, S^2 PLR-Homo3 uses three frozen GMT source hypotheses trained with different random seeds, and S^2 PLR-Hetero3 uses a heterogeneous frozen source committee composed of GMT, GIN, and PathNN. During target adaptation, all released source hypotheses are kept frozen and are used only for forward-pass reliability estimation, including pseudo-label prediction and predictive-variance computation. Gradients are propagated only through the target-side trainable modules. Therefore, increasing the number of source hypotheses affects the number of stored checkpoints and the forward-pass cost, but does not increase the number of trainable parameters optimized during adaptation.

The trainable parameter count of S^2 PLR comes from two target-side modules: the primary target model and the target-intrinsic structure encoder g_ψ . In our implementation, the primary target model is instantiated as GMT and is responsible for

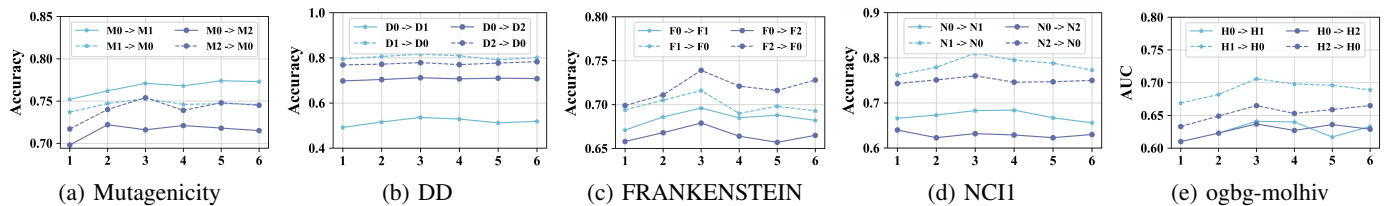


Fig. 7: Sensitivity analysis of the number of source experts K_e on Mutagenicity, DD, FRANKENSTEIN, NCII, and ogbg-molhiv.

TABLE XI: Time (in seconds) and GPU memory (in MB) consumption of different methods in the adaptation stage for each epoch.

Method	Source Hypotheses	Trainable Params	Adapt. Time	GPU Memory
GraphATA	1	164,738	0.9843	1,732
GALA	1	144,819	2.2843	5,530
GraphCTA	1	101,256	0.7563	1,312
SOGA	1	134,274	0.1873	1,678
S ² PLR-Single	1	445,828	1.7230	1,473
S ² PLR-Homo3	3	445,828	2.0377	1,614
S ² PLR-Hetero3	3	445,828	1.7617	5,665

target prediction and pseudo-label supervision, while g_ψ is instantiated as GIN and is used to learn target-intrinsic structural representations for graph contrastive learning and neighborhood-consistency verification. Both modules are updated during target adaptation. Thus, the trainable parameters of S²PLR correspond to the combination of the trainable GMT target model and the trainable GIN-based structure encoder, together with minor overhead from task-specific heads or projection layers. Importantly, this parameter count remains identical for S²PLR-Single, S²PLR-Homo3, and S²PLR-Hetero3, because the additional source hypotheses are frozen and never fine-tuned. The moderate runtime increase of the multi-hypothesis variants mainly comes from extra forward passes through frozen experts, while the higher memory usage of S²PLR-Hetero3 is due to the heterogeneous frozen encoders used during reliability estimation. Overall, the results show that the gains of S²PLR are not caused by additional trainable source models or test-time ensembling, but by using frozen source hypotheses to improve pseudo-label reliability, followed by target-structural verification and safe-subspace supervision.

G. Limitations

The proposed method has two limitations. First, the main version assumes that the source provider can release multiple source hypotheses or checkpoints. This is compatible with the source-free setting because no source graph is accessed during adaptation, but it may increase storage and inference cost. Second, the theoretical guarantee is selective: it applies to the safe subspace and does not certify correctness on all target samples. This is why uncertain samples are handled by soft regularization rather than hard pseudo-labels. These limitations are reflected in the design of the single-expert variant and the risk decomposition in Proposition 2.

TABLE XII: The results of ablation studies on the DD dataset (source \rightarrow target).

Methods	D0 \rightarrow D1	D1 \rightarrow D0	D0 \rightarrow D2	D2 \rightarrow D0	D0 \rightarrow D3	D3 \rightarrow D0	D1 \rightarrow D2	D2 \rightarrow D1	D1 \rightarrow D3	D3 \rightarrow D1	D2 \rightarrow D3	D3 \rightarrow D2
S ² PLR w/o ME	52.4	80.0	67.5	75.5	78.4	59.8	76.8	65.3	83.0	80.7	86.0	83.5
S ² PLR w/o CF	51.3	78.5	68.8	74.3	78.1	59.0	79.2	66.4	85.1	77.1	86.5	85.0
S ² PLR w/o TS	52.2	79.4	67.6	73.4	80.4	58.9	78.8	66.0	86.6	79.5	86.2	83.6
S ² PLR w/o NC	52.4	79.9	65.4	74.6	79.2	60.4	79.0	67.7	86.0	79.1	85.9	84.1
S ² PLR w/o SR	48.1	77.5	63.5	73.1	77.9	57.6	76.0	64.0	82.3	76.8	85.1	79.3
S ² PLR	55.7	80.5	70.1	77.3	82.7	62.8	81.4	68.1	87.3	83.2	88.0	86.7

TABLE XIII: The results of ablation studies on the FRANKENSTEIN dataset (source \rightarrow target).

Methods	F0 \rightarrow F1	F1 \rightarrow F0	F0 \rightarrow F2	F2 \rightarrow F0	F0 \rightarrow F3	F3 \rightarrow F0	F1 \rightarrow F2	F2 \rightarrow F1	F1 \rightarrow F3	F3 \rightarrow F1	F2 \rightarrow F3	F3 \rightarrow F2
S ² PLR w/o ME	67.1	66.1	65.2	71.7	57.2	55.3	59.1	69.6	57.1	64.5	57.7	67.3
S ² PLR w/o CF	67.7	68.2	64.6	70.2	55.1	56.2	66.7	68.4	56.9	62.4	59.4	66.9
S ² PLR w/o TS	67.6	64.2	62.9	71.5	56.2	54.7	66.1	68.1	57.3	64.9	58.9	68.7
S ² PLR w/o NC	67.8	67.5	63.7	69.9	53.1	54.0	67.5	67.5	55.2	62.2	58.1	67.1
S ² PLR w/o SR	67.4	58.0	55.7	61.7	49.1	43.2	58.5	67.9	53.7	59.1	57.5	63.9
S ² PLR	69.6	71.6	67.9	73.9	59.9	57.1	67.6	71.4	61.1	66.2	60.7	69.5

TABLE XIV: The results of ablation studies on the NCI1 dataset (source \rightarrow target).

Methods	N0 \rightarrow N1	N1 \rightarrow N0	N0 \rightarrow N2	N2 \rightarrow N0	N0 \rightarrow N3	N3 \rightarrow N0	N1 \rightarrow N2	N2 \rightarrow N1	N1 \rightarrow N3	N3 \rightarrow N1	N2 \rightarrow N3	N3 \rightarrow N2
S ² PLR w/o ME	66.8	77.1	62.0	72.6	65.9	70.9	68.8	72.3	67.9	61.4	72.9	69.6
S ² PLR w/o CF	67.1	78.6	62.3	74.6	65.2	69.1	71.1	75.5	68.0	62.1	76.2	72.7
S ² PLR w/o TS	66.9	79.9	61.4	73.6	65.5	67.5	70.0	74.8	67.8	62.3	75.8	71.7
S ² PLR w/o NC	66.0	78.3	61.8	72.0	66.8	68.6	70.3	75.3	66.9	61.6	75.5	71.5
S ² PLR w/o SR	59.6	76.5	60.0	70.9	65.3	63.8	69.3	71.4	67.5	54.1	70.1	68.3
S ² PLR	68.3	81.0	63.2	76.0	67.2	71.7	72.2	77.5	69.1	63.6	77.3	73.2

TABLE XV: The results of ablation studies on the ogbg-molhiv dataset (source \rightarrow target).

Methods	H0 \rightarrow H1	H1 \rightarrow H0	H0 \rightarrow H2	H2 \rightarrow H0	H0 \rightarrow H3	H3 \rightarrow H0	H1 \rightarrow H2	H2 \rightarrow H1	H1 \rightarrow H3	H3 \rightarrow H1	H2 \rightarrow H3	H3 \rightarrow H2
S ² PLR w/o ME	60.3	68.5	59.0	63.5	62.7	62.3	68.6	73.7	67.7	69.8	65.0	70.7
S ² PLR w/o CF	62.2	68.8	60.2	64.9	62.8	65.5	69.3	72.8	67.5	70.8	64.4	73.5
S ² PLR w/o TS	61.6	67.9	61.0	64.6	61.1	64.8	67.0	71.2	65.0	70.5	63.8	72.4
S ² PLR w/o NC	62.0	68.8	60.3	63.9	62.8	63.5	68.4	72.6	64.7	71.0	64.9	71.9
S ² PLR w/o SR	58.0	58.6	60.0	60.2	59.7	59.9	64.5	63.1	62.7	66.3	57.3	59.6
S ² PLR	64.1	70.6	63.7	66.5	64.6	66.1	70.2	74.4	70.8	73.4	68.0	76.2

TABLE XVI: The classification results (in %) on the DD dataset under node density domain shift (source \rightarrow target). D0, D1, D2, and D3 denote the sub-datasets partitioned with node density. **Bold** results indicate the best performance.

Methods	D0 \rightarrow D1	D1 \rightarrow D0	D0 \rightarrow D2	D2 \rightarrow D0	D0 \rightarrow D3	D3 \rightarrow D0	D1 \rightarrow D2	D2 \rightarrow D1	D1 \rightarrow D3	D3 \rightarrow D1	D2 \rightarrow D3	D3 \rightarrow D2
WL subtree	49.2	56.8	29.6	20.1	21.0	18.4	59.5	50.5	57.3	48.1	63.9	66.9
GCN	48.9 \pm 2.8	59.0 \pm 1.7	20.7 \pm 2.0	27.3 \pm 2.3	15.1 \pm 1.8	26.9 \pm 2.2	61.6 \pm 1.9	53.6 \pm 1.5	68.1 \pm 1.6	52.9 \pm 2.6	64.9 \pm 2.1	69.7 \pm 2.3
GIN	48.8 \pm 1.9	24.7 \pm 2.1	44.1 \pm 1.8	22.4 \pm 2.3	57.0 \pm 2.1	18.4 \pm 2.0	73.0 \pm 1.8	52.5 \pm 2.3	63.2 \pm 1.6	53.6 \pm 1.5	70.3 \pm 2.6	69.4 \pm 1.8
GMT	49.1 \pm 1.9	32.9 \pm 2.2	31.8 \pm 1.8	27.3 \pm 2.3	52.5 \pm 1.5	27.6 \pm 1.8	75.4 \pm 1.9	53.2 \pm 2.1	74.1 \pm 2.6	57.9 \pm 2.4	70.9 \pm 1.8	71.1 \pm 2.7
CIN	50.4 \pm 1.8	18.4 \pm 2.0	21.2 \pm 2.1	36.8 \pm 1.8	43.0 \pm 2.1	22.9 \pm 1.9	53.4 \pm 1.7	56.5 \pm 1.5	62.3 \pm 1.6	53.3 \pm 1.9	75.0 \pm 2.1	69.3 \pm 2.0
PathNN	50.1 \pm 2.3	58.8 \pm 2.0	31.6 \pm 2.1	28.6 \pm 1.6	21.6 \pm 2.1	30.3 \pm 1.3	69.1 \pm 2.3	59.5 \pm 1.4	74.5 \pm 2.4	57.8 \pm 1.9	74.9 \pm 1.8	71.1 \pm 1.6
SFDA_LLN	50.9 \pm 1.6	79.6 \pm 2.0	63.7 \pm 2.3	75.6 \pm 2.0	67.1 \pm 1.8	57.6 \pm 2.0	77.4 \pm 1.6	56.7 \pm 2.3	82.6 \pm 1.5	78.5 \pm 1.6	79.1 \pm 1.8	76.6 \pm 2.3
SF(DA) ²	51.3 \pm 1.4	78.4 \pm 2.1	63.8 \pm 1.3	76.6 \pm 2.3	68.6 \pm 2.3	59.7 \pm 2.3	75.7 \pm 1.6	57.4 \pm 1.6	81.4 \pm 1.9	79.1 \pm 2.6	80.7 \pm 2.0	77.8 \pm 1.7
NVC_LLN	49.7 \pm 2.0	79.4 \pm 1.5	64.7 \pm 1.7	78.0 \pm 1.9	68.5 \pm 2.3	59.3 \pm 1.7	76.2 \pm 2.1	58.1 \pm 1.8	82.3 \pm 1.6	77.8 \pm 2.0	80.3 \pm 2.1	76.7 \pm 1.8
Ucon_SFDA	51.5 \pm 1.9	80.6 \pm 2.2	66.7 \pm 1.4	72.3 \pm 1.8	69.1 \pm 0.9	58.8 \pm 2.1	78.1 \pm 0.6	60.6 \pm 3.1	83.6 \pm 0.4	79.2 \pm 0.7	82.2 \pm 1.6	79.5 \pm 1.0
SOGA	51.1 \pm 1.6	80.4 \pm 1.7	65.3 \pm 1.8	79.4 \pm 1.6	71.9 \pm 2.0	61.4 \pm 1.7	78.3 \pm 2.1	59.9 \pm 1.5	84.1 \pm 1.5	80.1 \pm 2.0	81.4 \pm 2.3	79.5 \pm 1.9
GraphCTA	50.9 \pm 1.5	81.2 \pm 2.4	67.7 \pm 2.0	79.5\pm2.3	70.9 \pm 2.2	62.3 \pm 1.5	79.5 \pm 1.7	61.9 \pm 1.9	85.1 \pm 2.0	80.9 \pm 2.1	82.1 \pm 2.0	78.3 \pm 1.7
GALA	52.8 \pm 1.7	80.8 \pm 2.1	66.0 \pm 2.1	77.2 \pm 2.0	71.4 \pm 1.9	60.8 \pm 1.8	78.5 \pm 1.4	60.8 \pm 1.7	84.4 \pm 1.6	81.2 \pm 1.2	83.6 \pm 2.5	77.6 \pm 2.3
GraphATA	51.7 \pm 1.4	80.3 \pm 3.2	67.6 \pm 2.4	78.4 \pm 1.9	72.1\pm1.3	63.8 \pm 1.5	78.7 \pm 2.3	67.8 \pm 2.3	84.1 \pm 0.9	81.5 \pm 1.2	85.7 \pm 1.0	81.2 \pm 1.2
S ² PLR	53.6\pm2.5	81.6\pm2.1	71.2\pm1.7	77.9 \pm 2.3	70.9 \pm 1.9	64.3\pm1.4	79.8\pm2.0	70.1\pm1.8	86.8\pm0.4	83.2\pm2.2	87.1\pm1.8	85.5\pm0.5

TABLE XVII: The classification results (in %) on the FRANKENSTEIN dataset under node density domain shift (source \rightarrow target). F0, F1, F2, and F3 denote the sub-datasets partitioned with node density. **Bold** results indicate the best performance.

Methods	F0 \rightarrow F1	F1 \rightarrow F0	F0 \rightarrow F2	F2 \rightarrow F0	F0 \rightarrow F3	F3 \rightarrow F0	F1 \rightarrow F2	F2 \rightarrow F1	F1 \rightarrow F3	F3 \rightarrow F1	F2 \rightarrow F3	F3 \rightarrow F2
WL subtree	54.6	40.1	47.8	62.0	49.6	56.0	49.7	51.2	41.8	42.9	47.3	45.1
GCN	32.7 \pm 2.0	43.2 \pm 2.1	42.2 \pm 1.7	43.2 \pm 1.5	54.5 \pm 1.8	43.2 \pm 1.9	42.2 \pm 2.0	32.7 \pm 1.5	56.5 \pm 1.2	32.7 \pm 1.8	55.5 \pm 1.8	42.2 \pm 2.0
GIN	39.7 \pm 1.8	51.4 \pm 1.7	54.7 \pm 1.3	51.4 \pm 1.7	58.2 \pm 1.9	41.8 \pm 2.0	54.7 \pm 2.3	47.1 \pm 1.6	52.1 \pm 1.2	34.3 \pm 1.5	50.8 \pm 1.7	43.8 \pm 2.0
GMT	47.3 \pm 2.2	56.8 \pm 1.9	57.8 \pm 1.4	56.8 \pm 1.2	39.5 \pm 2.3	44.1 \pm 1.2	57.8 \pm 2.0	58.3 \pm 1.5	39.5 \pm 1.6	39.3 \pm 1.4	39.5 \pm 2.0	44.1 \pm 1.6
CIN	54.3 \pm 1.8	51.6 \pm 1.9	45.0 \pm 1.7	52.5 \pm 1.8	51.9 \pm 2.1	43.2 \pm 2.0	45.3 \pm 1.3	60.4 \pm 1.8	48.8 \pm 1.6	32.7 \pm 2.0	57.1 \pm 1.2	42.2 \pm 1.8
PathNN	55.7 \pm 1.8	59.1 \pm 2.2	57.2 \pm 1.9	57.3 \pm 1.6	56.9 \pm 2.1	49.2 \pm 1.9	52.9 \pm 1.4	55.4 \pm 2.2	55.1 \pm 1.9	44.9 \pm 1.4	53.9 \pm 1.5	53.9 \pm 2.1
SFDA_LLN	65.2 \pm 1.3	59.2 \pm 2.2	59.1 \pm 1.0	58.9 \pm 2.1	57.6 \pm 1.2	59.9 \pm 1.9	59.4 \pm 1.3	65.0 \pm 1.5	58.3 \pm 2.0	64.9 \pm 1.8	57.5 \pm 1.3	58.4 \pm 1.9
SF(DA) ²	66.3 \pm 1.3	62.6 \pm 0.8	61.7 \pm 1.4	60.2 \pm 1.6	58.6 \pm 1.7	60.1 \pm 0.9	60.9 \pm 1.7	66.5 \pm 1.2	60.5 \pm 2.0	66.2 \pm 1.6	60.1 \pm 1.5	60.7 \pm 2.2
NVC_LLN	66.7 \pm 1.3	63.1 \pm 2.0	63.8 \pm 1.6	62.1 \pm 1.9	59.5 \pm 1.4	60.8 \pm 1.7	61.6 \pm 2.1	67.3 \pm 1.8	59.5 \pm 1.5	64.7 \pm 1.8	59.5 \pm 2.0	61.2 \pm 1.5
Ucon_SFDA	67.4 \pm 1.0	65.6 \pm 2.2	59.6 \pm 2.4	71.4 \pm 1.9	60.5 \pm 0.7	59.0 \pm 1.8	60.4 \pm 2.0	68.3 \pm 1.9	60.5 \pm 0.8	67.4\pm0.9	60.5 \pm 2.0	61.2 \pm 1.1
SOGA	67.0 \pm 1.7	63.8 \pm 1.3	65.2 \pm 1.5	63.7 \pm 1.6	60.3 \pm 1.7	60.2 \pm 1.6	62.2 \pm 1.9	67.7 \pm 2.0	61.0 \pm 1.5	66.9 \pm 1.2	60.6 \pm 1.8	61.3 \pm 2.3
GraphCTA	67.3 \pm 1.8	64.1 \pm 1.9	66.5 \pm 1.4	64.3 \pm 1.7	61.9 \pm 2.2	60.9 \pm 1.5	62.0 \pm 1.6	68.3 \pm 2.1	60.9 \pm 0.9	67.0 \pm 0.8	60.0 \pm 1.2	62.7 \pm 1.3
GALA	67.1 \pm 1.3	64.6 \pm 1.7	67.1 \pm 1.6	64.0 \pm 1.9	62.2\pm1.5	61.2 \pm 2.0	63.1 \pm 1.6	68.8 \pm 1.8	62.5\pm2.0	66.7 \pm 1.9	60.6 \pm 1.2	61.9 \pm 1.5
GraphATA	69.3 \pm 1.3	70.3 \pm 1.9	66.1 \pm 2.2	64.8 \pm 0.8	59.5 \pm 1.2	63.3\pm1.8	65.3 \pm 2.0	69.6 \pm 1.5	59.6 \pm 2.4	65.1 \pm 1.6	60.3 \pm 1.1	67.2 \pm 1.7
S ² PLR	69.6\pm1.8	71.6\pm2.1	67.9\pm2.4	73.9\pm1.6	59.9 \pm 1.6	57.1 \pm 2.0	67.6\pm1.2	71.4\pm2.2	61.1 \pm 1.3	66.2 \pm 2.9	60.7\pm1.4	69.5\pm1.6

TABLE XVIII: The classification results (in %) on the Mutagenicity dataset under node density domain shift (source \rightarrow target). M0, M1, M2, and M3 denote the sub-datasets partitioned with node density. **Bold** results indicate the best performance.

Methods	M0 \rightarrow M1	M1 \rightarrow M0	M0 \rightarrow M2	M2 \rightarrow M0	M0 \rightarrow M3	M3 \rightarrow M0	M1 \rightarrow M2	M2 \rightarrow M1	M1 \rightarrow M3	M3 \rightarrow M1	M2 \rightarrow M3	M3 \rightarrow M2
WL subtree	34.3	46.0	40.4	50.4	52.7	52.1	51.6	48.3	45.6	40.8	53.5	52.4
GCN	64.1 \pm 1.4	62.6 \pm 2.3	65.5 \pm 2.0	62.3 \pm 1.1	56.9 \pm 2.1	53.7 \pm 1.8	66.1 \pm 1.6	70.8 \pm 2.1	47.7 \pm 1.9	49.2 \pm 2.1	52.1 \pm 1.7	54.4 \pm 2.1
GIN	66.5 \pm 2.1	53.2 \pm 2.3	52.0 \pm 1.7	62.6 \pm 2.3	53.7 \pm 1.7	48.6 \pm 2.3	71.5 \pm 2.5	70.0 \pm 2.1	52.2 \pm 2.3	64.3 \pm 2.1	50.9 \pm 1.4	52.4 \pm 1.5
GMT	65.7 \pm 1.8	67.1 \pm 1.9	62.1 \pm 2.1	66.4 \pm 1.2	59.0 \pm 2.0	58.0 \pm 2.7	69.9 \pm 1.4	68.4 \pm 2.3	60.4 \pm 1.3	48.2 \pm 2.0	59.1 \pm 1.3	60.6 \pm 1.7
CIN	65.1 \pm 1.7	52.9 \pm 2.3	66.0 \pm 1.7	69.8 \pm 2.0	55.2 \pm 1.5	55.1 \pm 1.3	66.0 \pm 1.6	69.9 \pm 2.1	54.9 \pm 1.8	57.8 \pm 1.5	46.7 \pm 2.0	51.8 \pm 1.1
PathNN	70.2 \pm 1.5	68.9 \pm 1.5	67.1 \pm 2.0	70.2 \pm 1.3	58.0 \pm 1.9	60.4 \pm 2.2	68.9 \pm 1.6	70.3 \pm 1.9	59.8 \pm 1.7	57.7 \pm 1.5	59.9 \pm 1.7	61.8 \pm 0.9
SFDA_LLN	70.7 \pm 1.6	69.2 \pm 2.3	68.1 \pm 1.2	67.9 \pm 2.3	60.4 \pm 1.3	61.4 \pm 1.9	70.8 \pm 1.7	74.1 \pm 1.6	60.1 \pm 1.1	68.8 \pm 1.4	59.3 \pm 2.1	65.4 \pm 2.3
SF(DA) ²	72.0 \pm 1.5	69.6 \pm 1.5	69.7 \pm 1.9	70.7 \pm 2.1	62.0 \pm 1.8	61.9 \pm 3.2	73.1 \pm 1.7	75.9 \pm 1.5	63.4 \pm 1.8	69.8 \pm 2.0	63.9 \pm 1.9	68.9 \pm 1.7
NVC_LLN	71.4 \pm 1.3	70.2 \pm 1.4	67.8 \pm 1.1	70.9 \pm 2.3	62.1 \pm 1.5	63.2 \pm 1.7	72.3 \pm 1.6	75.8 \pm 1.6	62.7 \pm 2.1	69.0 \pm 1.4	62.0 \pm 2.3	65.2 \pm 2.5
Ucon_SFDA	73.2 \pm 0.8	72.7 \pm 1.3	69.6 \pm 2.1	70.6 \pm 1.0	62.9 \pm 3.2	62.8 \pm 1.8	72.2 \pm 1.9	76.0 \pm 0.9	63.8 \pm 1.2	67.3 \pm 1.5	61.3 \pm 0.7	66.4 \pm 1.7
SOGA	73.5 \pm 1.3	69.9 \pm 2.0	69.4 \pm 2.5	71.0 \pm 2.0	63.1 \pm 2.1	64.6 \pm 1.7	73.8 \pm 1.3	75.5 \pm 2.0	65.0 \pm 1.5	76.4 \pm 1.4	63.5 \pm 1.8	71.6 \pm 2.0
GraphCTA	73.7 \pm 1.8	70.5 \pm 2.0	70.7 \pm 1.5	71.7 \pm 1.7	65.2 \pm 1.7	66.7 \pm 2.1	73.1 \pm 1.6	76.1 \pm 1.9	64.7 \pm 2.0	75.6 \pm 1.4	63.9 \pm 1.7	73.7 \pm 1.9
GALA	75.1 \pm 2.1	71.3 \pm 1.7	70.8 \pm 1.6	72.8 \pm 1.5	64.0 \pm 2.1	66.0 \pm 1.6	72.6 \pm 1.8	76.5 \pm 2.3	65.3 \pm 1.4	76.9 \pm 1.5	64.4 \pm 2.4	74.5 \pm 1.1
GraphATA	75.2 \pm 2.1	73.0 \pm 1.7	69.9 \pm 1.3	70.7 \pm 1.0	62.1 \pm 1.0	70.7 \pm 1.0	73.7 \pm 2.2	76.0 \pm 1.2	68.9 \pm 1.2	80.2 \pm 1.8	64.3 \pm 0.7	73.3 \pm 2.0
S ² PLR	77.1\pm0.5	75.3\pm0.7	71.6\pm2.0	75.4\pm0.4	65.8\pm1.1	72.0\pm1.4	79.9\pm0.6	87.2\pm0.4	70.8\pm0.6	82.4\pm0.3	71.9\pm1.5	81.6\pm2.3

TABLE XIX: The classification results (in %) on the NCI1 dataset under node density domain shift (source \rightarrow target). N0, N1, N2, and N3 denote the sub-datasets partitioned with node density. **Bold** results indicate the best performance.

Methods	N0 \rightarrow N1	N1 \rightarrow N0	N0 \rightarrow N2	N2 \rightarrow N0	N0 \rightarrow N3	N3 \rightarrow N0	N1 \rightarrow N2	N2 \rightarrow N1	N1 \rightarrow N3	N3 \rightarrow N1	N2 \rightarrow N3	N3 \rightarrow N2
WL subtree	54.9	60.0	51.4	51.4	44.4	63.1	51.9	53.4	58.4	57.4	61.2	50.9
GCN	54.0 \pm 2.0	66.5 \pm 1.9	47.3 \pm 2.2	37.4 \pm 1.8	38.4 \pm 2.3	27.6 \pm 1.5	59.0 \pm 1.7	56.9 \pm 2.0	56.5 \pm 1.2	51.0 \pm 1.7	60.5 \pm 1.9	57.4 \pm 1.6
GIN	57.0 \pm 1.9	38.7 \pm 2.3	45.7 \pm 1.8	34.4 \pm 1.9	43.6 \pm 2.1	27.0 \pm 2.0	54.7 \pm 1.7	52.8 \pm 2.1	59.0 \pm 1.8	49.1 \pm 2.5	59.4 \pm 2.0	57.4 \pm 1.3
GMT	53.0 \pm 1.9	63.7 \pm 1.6	48.9 \pm 2.2	32.8 \pm 2.0	41.5 \pm 1.7	27.8 \pm 1.6	56.4 \pm 1.9	57.2 \pm 1.7	54.1 \pm 1.9	49.8 \pm 1.7	61.6 \pm 2.1	58.5 \pm 1.1
CIN	54.5 \pm 1.9	37.6 \pm 1.9	53.2 \pm 1.8	36.2 \pm 1.4	42.1 \pm 1.8	27.5 \pm 2.0	57.2 \pm 1.6	51.6 \pm 1.9	59.3 \pm 1.5	50.0 \pm 1.4	62.0 \pm 1.4	57.4 \pm 2.3
PathNN	56.8 \pm 2.5	62.8 \pm 2.1	52.7 \pm 2.2	64.5 \pm 1.2	50.6 \pm 1.8	37.4 \pm 2.1	59.2 \pm 1.4	58.6 \pm 1.5	60.2 \pm 1.8	53.1 \pm 2.1	60.9 \pm 1.2	57.6 \pm 1.5
SFDA_LLN	56.4 \pm 2.0	71.1 \pm 1.8	55.7 \pm 1.5	73.0 \pm 2.0	66.4 \pm 1.2	72.6 \pm 1.8	57.4 \pm 1.2	59.0 \pm 2.1	65.5 \pm 2.0	54.4 \pm 1.8	64.5 \pm 2.0	59.4 \pm 1.4
SF(DA) ²	57.2 \pm 1.9	72.7 \pm 2.1	56.3 \pm 1.9	72.9 \pm 1.5	65.7 \pm 1.5	72.3 \pm 2.0	59.7 \pm 1.8	61.0 \pm 1.9	65.2 \pm 2.0	57.5 \pm 1.3	65.2 \pm 1.7	60.7 \pm 1.3
NVC_LLN	58.9 \pm 2.0	72.0 \pm 1.8	56.7 \pm 1.9	73.1 \pm 1.6	65.2 \pm 2.3	71.0 \pm 2.1	61.4 \pm 1.8	62.1 \pm 1.4	66.3 \pm 1.2	59.1 \pm 1.6	65.9 \pm 2.0	63.3 \pm 1.9
Ucon_SFDA	61.9 \pm 1.2	73.8 \pm 0.7	58.6 \pm 2.5	72.7 \pm 1.3	64.8 \pm 1.3	71.8 \pm 1.8	58.1 \pm 0.8	61.4 \pm 2.9	66.8 \pm 0.5	59.7 \pm 3.1	66.9 \pm 0.8	57.5 \pm 1.1
SOGA	61.0 \pm 1.5	73.1 \pm 2.1	58.0 \pm 1.4	73.0 \pm 1.0	66.3 \pm 1.3	72.8 \pm 1.6	63.5 \pm 2.2	64.1 \pm 1.8	66.5 \pm 2.0	59.9 \pm 1.6	66.5 \pm 1.7	64.0 \pm 2.0
GraphCTA	60.9 \pm 2.0	73.7 \pm 1.6	58.7 \pm 1.8	74.2 \pm 1.4	65.9 \pm 1.8	72.0 \pm 2.0	64.4 \pm 0.9	63.3 \pm 1.2	67.3 \pm 1.5	59.1 \pm 2.0	65.8 \pm 1.6	63.9 \pm 2.1
GALA	61.2 \pm 1.3	73.4 \pm 1.4	58.4 \pm 1.8	74.8 \pm 2.0	68.5\pm1.5	73.7\pm1.8	64.8 \pm 1.2	64.4 \pm 2.0	67.5 \pm 1.5	58.9 \pm 0.9	66.6 \pm 1.0	64.0 \pm 2.2
GraphATA	63.9 \pm 0.8	74.5 \pm 2.0	57.7 \pm 1.9	74.4 \pm 2.6	68.1 \pm 1.8	71.9 \pm 0.8	66.0 \pm 1.3	62.4 \pm 1.7	64.6 \pm 2.0	59.6 \pm 1.6	69.5 \pm 1.0	68.2 \pm 0.4
S ² PLR	68.3\pm1.5	81.0\pm2.4	63.2\pm1.6	76.0\pm2.0	67.2 \pm 1.4	71.7 \pm 1.9	72.2\pm1.1	77.5\pm1.2	69.1\pm0.3	63.6\pm0.9	77.3\pm1.2	73.2\pm2.4

TABLE XX: ROC-AUC results (in %) on the ogbg-molhiv dataset under node density domain shift (source \rightarrow target). H0, H1, H2, and H3 denote the sub-datasets partitioned with node density. **Bold** results indicate the best performance.

Methods	H0 \rightarrow H1	H1 \rightarrow H0	H0 \rightarrow H2	H2 \rightarrow H0	H0 \rightarrow H3	H3 \rightarrow H0	H1 \rightarrow H2	H2 \rightarrow H1	H1 \rightarrow H3	H3 \rightarrow H1	H2 \rightarrow H3	H3 \rightarrow H2
WL	49.6	51.8	54.0	54.7	48.2	48.9	50.6	51.9	38.1	51.0	51.8	50.7
GCN	57.8 \pm 1.9	57.4 \pm 2.1	56.5 \pm 1.3	54.2 \pm 1.2	54.5 \pm 1.7	51.9 \pm 1.7	61.8 \pm 2.0	55.2 \pm 1.3	49.8 \pm 1.4	56.6 \pm 1.3	61.5 \pm 1.1	56.8 \pm 1.7
GIN	59.1 \pm 1.6	53.3 \pm 1.6	50.0 \pm 1.7	54.8 \pm 1.8	56.8 \pm 1.6	50.7 \pm 1.4	55.2 \pm 1.3	58.7 \pm 1.4	57.0 \pm 1.8	49.6 \pm 1.7	53.1 \pm 1.3	55.3 \pm 1.6
GMT	51.1 \pm 1.6	57.2 \pm 1.7	50.6 \pm 1.2	55.9 \pm 1.9	58.4 \pm 1.4	53.4 \pm 1.7	56.1 \pm 1.6	57.6 \pm 1.3	60.9 \pm 1.7	54.5 \pm 2.0	55.4 \pm 1.6	51.2 \pm 1.8
CIN	52.3 \pm 1.6	53.4 \pm 1.5	54.0 \pm 1.9	57.5 \pm 1.8	56.5 \pm 1.4	51.1 \pm 1.9	55.8 \pm 1.4	63.6 \pm 1.8	48.7 \pm 1.6	56.8 \pm 1.6	49.3 \pm 1.2	52.8 \pm 1.3
PathNN	50.3 \pm 1.3	51.2 \pm 1.8	51.5 \pm 1.2	55.3 \pm 1.8	56.7 \pm 1.2	52.2 \pm 1.5	53.7 \pm 1.7	51.5 \pm 1.4	53.9 \pm 1.9	54.3 \pm 1.5	55.6 \pm 1.8	56.0 \pm 1.5
SFDA_LLN	63.1 \pm 1.1	63.8 \pm 1.6	62.9 \pm 1.5	62.9 \pm 1.6	63.9 \pm 0.9	62.4 \pm 1.6	63.5 \pm 1.4	64.7 \pm 1.3	63.9 \pm 1.7	61.3 \pm 1.7	66.2 \pm 1.6	60.9 \pm 1.1
SF(DA) ²	63.3 \pm 1.5	63.7 \pm 1.4	62.7 \pm 1.4	63.4 \pm 1.3	64.1 \pm 1.3	60.4 \pm 2.4	64.5 \pm 1.0	64.9 \pm 1.6	64.2 \pm 1.4	61.6 \pm 1.3	64.2 \pm 1.3	61.6 \pm 1.9
NVC_LLN	57.2 \pm 0.4	61.8 \pm 0.4	58.3 \pm 0.3	61.7 \pm 0.4	61.9 \pm 1.6	61.4 \pm 1.0	60.3 \pm 1.5	58.2 \pm 1.7	64.1 \pm 1.7	60.4 \pm 1.8	62.3 \pm 2.5	60.0 \pm 1.1
Ucon_SFDA	60.4 \pm 0.9	63.2 \pm 1.3	61.1 \pm 1.8	63.4 \pm 0.5	62.0 \pm 1.2	62.1 \pm 0.7	61.8 \pm 1.1	64.1 \pm 0.7	63.5 \pm 0.5	62.4 \pm 1.0	62.3 \pm 0.6	63.4 \pm 1.0
SOGA	62.8 \pm 1.6	62.3 \pm 1.3	63.2 \pm 1.9	62.1 \pm 1.8	63.8 \pm 1.6	64.1 \pm 1.2	63.2 \pm 2.9	66.8 \pm 1.6	67.2 \pm 2.3	61.8 \pm 1.3	65.4 \pm 2.1	63.7 \pm 1.7
GraphCTA	63.7 \pm 1.4	65.5 \pm 1.4	63.8 \pm 1.2	63.0 \pm 1.6	64.3 \pm 1.2	63.1 \pm 2.3	65.4 \pm 1.4	67.0 \pm 1.7	65.2 \pm 1.5	62.8 \pm 1.5	67.9 \pm 1.9	63.3 \pm 1.8
GALA	63.5 \pm 1.4	64.9 \pm 1.9	64.3\pm1.6	63.8 \pm 1.2	64.4 \pm 1.4	64.3 \pm 1.5	65.0 \pm 1.9	67.7 \pm 1.2	69.1 \pm 1.4	63.9 \pm 1.1	68.5\pm1.3	64.3 \pm 1.6
GraphATA	63.0 \pm 0.9	68.2 \pm 0.5	62.5 \pm 0.7	62.5 \pm 1.7	62.4 \pm 1.4	65.0 \pm 1.0	64.7 \pm 2.0	68.9 \pm 1.3	69.2 \pm 2.3	65.1 \pm 1.2	66.8 \pm 1.0	69.3 \pm 0.7
S ² PLR	64.1\pm1.4	70.6\pm1.8	63.7 \pm 1.6	66.5\pm2.6	64.6\pm1.9	66.1\pm2.1	70.2\pm3.1	74.4\pm2.7	70.8\pm2.3	73.4\pm0.8	68.0 \pm 3.1	76.2\pm0.7

TABLE XXI: The classification results (in %) on the DD dataset under edge density domain shift (source \rightarrow target). D0, D1, D2, and D3 denote the sub-datasets partitioned with edge density. **Bold** results indicate the best performance.

Methods	D0 \rightarrow D1	D1 \rightarrow D0	D0 \rightarrow D2	D2 \rightarrow D0	D0 \rightarrow D3	D3 \rightarrow D0	D1 \rightarrow D2	D2 \rightarrow D1	D1 \rightarrow D3	D3 \rightarrow D1	D2 \rightarrow D3	D3 \rightarrow D2
WL subtree	49.2	56.8	29.6	20.1	21.0	18.4	59.5	50.5	57.3	48.1	63.9	66.9
GCN	48.9 \pm 2.8	59.0 \pm 1.7	20.7 \pm 2.0	27.3 \pm 2.3	15.1 \pm 1.8	26.9 \pm 2.2	61.6 \pm 1.9	53.6 \pm 1.5	68.1 \pm 1.6	52.9 \pm 2.6	64.9 \pm 2.1	69.7 \pm 2.3
GIN	48.8 \pm 1.9	24.7 \pm 2.1	44.1 \pm 1.8	22.4 \pm 2.3	57.0 \pm 2.1	18.4 \pm 2.0	73.0 \pm 1.8	52.5 \pm 2.3	63.2 \pm 1.6	53.6 \pm 1.5	70.3 \pm 2.6	69.4 \pm 1.8
GMT	49.1 \pm 1.9	32.9 \pm 2.2	31.8 \pm 1.8	27.3 \pm 2.3	52.5 \pm 1.5	27.6 \pm 1.8	75.4 \pm 1.9	53.2 \pm 2.1	74.1 \pm 2.6	57.9 \pm 2.4	70.9 \pm 1.8	71.1 \pm 2.7
CIN	50.4 \pm 1.8	18.4 \pm 2.0	21.2 \pm 2.1	36.8 \pm 1.8	43.0 \pm 2.1	22.9 \pm 1.9	53.4 \pm 1.7	56.5 \pm 1.5	62.3 \pm 1.6	53.3 \pm 1.9	75.0 \pm 2.1	69.3 \pm 2.0
PathNN	50.0 \pm 2.1	59.9 \pm 1.7	42.0 \pm 2.3	43.5 \pm 1.4	31.7 \pm 1.7	37.6 \pm 2.3	66.5 \pm 1.6	54.1 \pm 1.7	69.2 \pm 1.9	56.1 \pm 1.8	74.7 \pm 1.8	69.5 \pm 1.0
SFDA_LLN	51.4 \pm 2.2	75.9 \pm 1.8	72.0 \pm 2.1	75.3 \pm 2.3	82.3 \pm 2.3	56.7 \pm 1.8	74.1 \pm 1.2	53.8 \pm 1.9	82.5 \pm 1.5	79.5 \pm 1.6	72.2 \pm 2.1	70.1 \pm 1.9
SF(DA) ²	51.9 \pm 2.3	77.7 \pm 2.6	72.4 \pm 1.2	74.5 \pm 1.9	82.5 \pm 1.4	58.4 \pm 1.8	75.9 \pm 1.6	53.7 \pm 2.2	83.7 \pm 2.2	81.4 \pm 2.0	74.4 \pm 2.4	72.8 \pm 1.8
NVC_LLN	51.5 \pm 2.0	77.0 \pm 1.9	71.1 \pm 1.8	75.5 \pm 1.7	82.5 \pm 2.1	60.2 \pm 1.7	75.3 \pm 1.8	53.8 \pm 2.5	82.1 \pm 2.2	79.8 \pm 2.4	74.7 \pm 1.2	70.5 \pm 2.0
Ucon_SFDA	52.2 \pm 1.3	80.7 \pm 2.0	77.5 \pm 0.9	75.9 \pm 2.6	86.6 \pm 0.8	60.1 \pm 1.4	79.9 \pm 1.8	59.8 \pm 2.9	83.8 \pm 1.2	79.6 \pm 1.3	79.2 \pm 1.4	72.6 \pm 0.6
SOGA	52.1 \pm 1.4	79.4 \pm 1.7	73.3 \pm 0.9	78.4 \pm 1.8	83.9 \pm 2.0	57.4 \pm 1.8	78.2 \pm 1.6	55.9 \pm 2.0	84.3 \pm 2.4	84.0 \pm 2.0	76.1 \pm 2.1	73.1 \pm 1.7
GraphCTA	51.9 \pm 1.5	79.8 \pm 2.1	73.8 \pm 2.0	77.6 \pm 2.5	85.4 \pm 1.9	56.1 \pm 1.8	77.5 \pm 2.4	56.9 \pm 2.0	85.1 \pm 1.7	83.9 \pm 2.0	75.1 \pm 2.3	72.2 \pm 1.9
GALA	52.3 \pm 1.6	80.2 \pm 1.9	74.6\pm2.0	78.4 \pm 1.7	84.8 \pm 1.5	60.9 \pm 2.1	78.0 \pm 1.7	57.7 \pm 1.9	85.5 \pm 2.3	87.1\pm1.4	78.2 \pm 2.4	74.5 \pm 1.8
GraphATA	52.5 \pm 0.8	80.0 \pm 2.4	73.6 \pm 3.0	79.5\pm1.8	86.5\pm2.1	57.3 \pm 1.9	80.5 \pm 1.9	66.4 \pm 1.8	85.5 \pm 0.9	87.4 \pm 1.4	82.3 \pm 1.1	80.4 \pm 2.1
S ² PLR	55.7\pm2.1	80.5\pm2.3	70.1 \pm 2.0	77.3 \pm 1.4	82.7 \pm 1.2	62.8\pm1.4	81.4\pm3.8	68.1\pm3.1	87.3\pm1.2	83.2 \pm 1.7	88.0\pm0.8	86.7\pm1.4

TABLE XXII: The classification results (in %) on the FRANKENSTEIN dataset under edge density domain shift (source \rightarrow target). F0, F1, F2, and F3 denote the sub-datasets partitioned with edge density. **Bold** results indicate the best performance.

Methods	F0 \rightarrow F1	F1 \rightarrow F0	F0 \rightarrow F2	F2 \rightarrow F0	F0 \rightarrow F3	F3 \rightarrow F0	F1 \rightarrow F2	F2 \rightarrow F1	F1 \rightarrow F3	F3 \rightarrow F1	F2 \rightarrow F3	F3 \rightarrow F2
WL subtree	44.6	54.8	47.0	56.1	58.2	41.8	50.8	58.1	45.7	47.9	45.3	42.7
GCN	33.5 \pm 2.1	40.9 \pm 1.5	44.6 \pm 1.3	40.1 \pm 1.6	57.4 \pm 2.0	43.1 \pm 1.3	44.6 \pm 2.0	33.5 \pm 1.2	56.4 \pm 1.1	36.6 \pm 1.9	57.4 \pm 2.0	47.8 \pm 1.7
GIN	40.1 \pm 1.2	52.4 \pm 1.8	52.2 \pm 2.2	52.7 \pm 1.8	58.3 \pm 1.5	42.8 \pm 2.0	53.2 \pm 2.3	47.1 \pm 1.6	52.1 \pm 2.2	39.1 \pm 2.0	49.9 \pm 1.8	43.5 \pm 1.9
GMT	51.5 \pm 1.0	57.0 \pm 1.3	55.4 \pm 1.6	59.0 \pm 1.2	39.6 \pm 1.6	44.1 \pm 2.0	55.4 \pm 2.1	66.5 \pm 1.6	39.6 \pm 1.9	36.5 \pm 1.5	39.6 \pm 1.4	42.8 \pm 1.4
CIN	54.2 \pm 1.1	52.2 \pm 1.9	47.6 \pm 1.8	52.5 \pm 2.2	56.2 \pm 1.3	40.0 \pm 2.0	46.8 \pm 1.3	59.9 \pm 1.2	49.1 \pm 1.5	33.5 \pm 2.0	57.8 \pm 1.4	45.9 \pm 2.0
PathNN	55.9 \pm 1.5	59.6 \pm 1.7	56.5 \pm 1.5	60.8 \pm 1.6	57.0 \pm 1.2	48.0 \pm 1.7	49.2 \pm 1.3	60.2 \pm 1.9	55.1 \pm 1.5	48.2 \pm 1.8	54.1 \pm 1.9	54.1 \pm 2.2
SFDA_LLN	64.6 \pm 1.3	62.5 \pm 2.7	55.3 \pm 1.9	60.9 \pm 1.8	60.6 \pm 1.2	63.5 \pm 2.1	55.6 \pm 1.3	66.7 \pm 1.3	60.4 \pm 1.8	56.8 \pm 1.7	60.4 \pm 2.0	55.4 \pm 1.1
SF(DA) ²	65.1 \pm 1.4	64.5 \pm 1.1	57.4 \pm 1.5	60.3 \pm 2.0	59.1 \pm 2.2	64.4 \pm 1.8	57.7 \pm 1.2	67.0 \pm 1.3	60.1 \pm 2.0	59.2 \pm 1.5	58.9 \pm 2.1	58.1 \pm 1.2
NVC_LLN	65.5 \pm 1.3	65.0 \pm 0.9	57.0 \pm 1.2	61.0 \pm 2.1	59.6 \pm 1.6	63.0 \pm 1.7	57.4 \pm 1.4	66.5 \pm 2.0	59.6 \pm 1.4	58.5 \pm 1.9	59.6 \pm 1.7	61.6 \pm 2.1
Ucon_SFDA	68.0 \pm 0.6	69.0 \pm 2.1	55.6 \pm 1.7	60.2 \pm 2.2	60.4 \pm 1.5	61.6 \pm 1.4	55.8 \pm 0.9	66.9 \pm 0.7	58.0 \pm 2.5	60.0 \pm 1.6	60.4 \pm 2.0	59.7 \pm 2.3
SOGA	63.5 \pm 1.8	65.1 \pm 1.4	58.4 \pm 0.8	60.8 \pm 1.2	58.8 \pm 1.1	64.4 \pm 2.0	60.7 \pm 1.6	68.5 \pm 1.3	60.6 \pm 1.6	59.4 \pm 2.1	60.2 \pm 1.4	63.8 \pm 1.3
GraphCTA	66.4 \pm 1.9	66.7 \pm 1.4	60.4 \pm 1.3	61.7 \pm 1.3	59.9 \pm 1.2	64.3 \pm 2.0	62.3 \pm 1.6	67.9 \pm 1.4	60.4 \pm 2.0	58.8 \pm 1.2	60.5 \pm 1.8	62.9 \pm 2.1
GALA	65.9 \pm 1.7	67.0 \pm 1.3	61.3 \pm 2.0	62.0 \pm 2.1	60.5 \pm 2.5	64.8 \pm 1.7	63.0 \pm 2.1	66.9 \pm 1.6	60.6 \pm 1.8	59.0 \pm 1.9	59.7 \pm 2.2	63.3 \pm 1.8
GraphATA	65.7 \pm 1.2	66.8 \pm 0.9	63.4 \pm 2.0	68.0 \pm 1.8	61.3\pm2.3	65.5\pm0.6	65.4 \pm 1.7	68.8 \pm 1.5	59.6 \pm 1.3	60.5\pm1.7	61.0 \pm 3.1	64.6 \pm 1.0
S ² PLR	72.5\pm0.9	76.0\pm2.9	65.8\pm1.8	75.5\pm2.4	58.5 \pm 1.7	63.8 \pm 1.1	66.2\pm2.9	79.6\pm2.7	60.9\pm2.3	58.7 \pm 1.8	62.2\pm1.6	72.7\pm1.9

TABLE XXIII: The classification results (in %) on the Mutagenicity dataset under edge density domain shift (source \rightarrow target). M0, M1, M2, and M3 denote the sub-datasets partitioned with edge density. **Bold** results indicate the best performance.

Methods	M0 \rightarrow M1	M1 \rightarrow M0	M0 \rightarrow M2	M2 \rightarrow M0	M0 \rightarrow M3	M3 \rightarrow M0	M1 \rightarrow M2	M2 \rightarrow M1	M1 \rightarrow M3	M3 \rightarrow M1	M2 \rightarrow M3	M3 \rightarrow M2
WL subtree	34.4	39.6	47.6	43.6	52.7	46.4	59.8	40.9	53.0	65.1	52.6	42.4
GCN	66.3 \pm 1.7	65.1 \pm 2.2	63.6 \pm 1.4	67.6 \pm 1.6	56.0 \pm 1.4	49.6 \pm 1.9	66.1 \pm 2.0	71.8 \pm 1.8	48.0 \pm 2.3	47.8 \pm 1.7	51.6 \pm 1.8	56.6 \pm 2.2
GIN	67.1 \pm 1.7	56.1 \pm 1.5	54.2 \pm 2.6	65.6 \pm 1.6	55.4 \pm 1.9	50.8 \pm 2.1	67.9 \pm 2.1	69.4 \pm 2.0	53.4 \pm 1.6	66.7 \pm 2.0	50.4 \pm 1.1	55.4 \pm 1.2
GMT	67.9 \pm 1.3	63.9 \pm 1.8	61.5 \pm 1.8	68.5 \pm 1.5	58.2 \pm 2.4	54.3 \pm 1.8	66.7 \pm 1.9	76.1 \pm 1.7	58.8 \pm 1.5	44.5 \pm 1.5	59.0 \pm 1.4	63.7 \pm 1.7
CIN	66.3 \pm 1.8	56.7 \pm 2.5	60.8 \pm 1.7	67.4 \pm 1.7	55.8 \pm 2.4	52.3 \pm 1.8	63.4 \pm 2.3	69.3 \pm 1.2	54.3 \pm 1.2	60.7 \pm 1.4	49.0 \pm 1.3	54.4 \pm 1.7
PathNN	68.9 \pm 1.9	65.9 \pm 1.8	62.9 \pm 1.7	69.2 \pm 1.8	58.1 \pm 1.6	59.9 \pm 1.4	67.7 \pm 1.6	70.0 \pm 2.1	56.3 \pm 1.8	62.8 \pm 1.9	59.2 \pm 1.6	63.7 \pm 1.2
SFDA_LLN	67.7 \pm 1.5	70.0 \pm 2.1	66.5 \pm 2.6	70.2 \pm 1.9	58.8 \pm 2.1	64.3 \pm 2.4	69.8 \pm 2.0	74.1 \pm 2.0	63.2 \pm 1.7	71.5 \pm 1.2	61.4 \pm 2.0	67.1 \pm 1.9
SF(DA) ²	71.7 \pm 1.9	70.7 \pm 1.4	68.8 \pm 2.3	70.4 \pm 2.2	61.9 \pm 2.0	66.4 \pm 1.9	70.8 \pm 1.7	73.9 \pm 1.7	63.1 \pm 1.5	72.1 \pm 1.8	64.8 \pm 1.4	71.8 \pm 1.5
NVC_LLN	70.4 \pm 2.2	69.1 \pm 1.5	67.0 \pm 2.2	70.8 \pm 2.5	62.2 \pm 1.7	68.3 \pm 1.9	70.3 \pm 2.4	76.3 \pm 1.5	63.0 \pm 1.8	69.5 \pm 2.5	63.9 \pm 1.3	68.0 \pm 2.1
Ucon_SFDA	74.1 \pm 1.1	74.1 \pm 0.6	68.2 \pm 1.2	72.5 \pm 0.4	63.5 \pm 3.7	72.4 \pm 1.8	71.1 \pm 1.0	74.6 \pm 2.1	63.9 \pm 2.3	72.7 \pm 1.3	63.3 \pm 0.9	67.2 \pm 1.6
SOGA	72.3 \pm 2.2	72.1 \pm 1.5	69.8 \pm 1.9	72.8 \pm 1.4	63.1 \pm 1.8	71.2 \pm 1.6	69.2 \pm 1.9	76.7 \pm 1.7	62.9 \pm 1.9	75.5 \pm 1.7	65.5 \pm 1.9	73.5 \pm 1.7
GraphCTA	72.0 \pm 2.2	71.4 \pm 2.0	70.5\pm1.6	72.9 \pm 1.8	62.8 \pm 1.8	71.7 \pm 2.2	70.1 \pm 1.7	76.5 \pm 1.8	64.4 \pm 1.6	77.8 \pm 2.0	65.8 \pm 2.1	73.6 \pm 1.8
GALA	72.2 \pm 1.2	73.3 \pm 1.0	70.3 \pm 1.7	72.3 \pm 2.2	63.4 \pm 1.8	69.7 \pm 1.4	72.7 \pm 1.7	74.9 \pm 1.5	65.5 \pm 1.9	76.7 \pm 1.7	65.1 \pm 1.5	73.0 \pm 1.7
GraphATA	74.4 \pm 1.3	74.4 \pm 1.1	69.0 \pm 0.9	71.8 \pm 1.9	61.9 \pm 2.2	72.8 \pm 1.3	73.1 \pm 0.8	74.7 \pm 1.3	67.5 \pm 2.2	76.1 \pm 1.7	68.1 \pm 1.6	74.7 \pm 1.0
S ² PLR	75.8\pm2.1	78.1\pm1.0	69.9 \pm 1.6	78.3\pm0.2	66.2\pm1.4	74.5\pm1.9	77.7\pm1.7	85.6\pm0.3	67.2\pm1.6	78.6\pm2.0	72.5\pm0.4	81.1\pm0.7

TABLE XXIV: The classification results (in %) on the NCI1 dataset under edge density domain shift (source \rightarrow target). N0, N1, N2, and N3 denote the sub-datasets partitioned with edge density. **Bold** results indicate the best performance.

Methods	N0 \rightarrow N1	N1 \rightarrow N0	N0 \rightarrow N2	N2 \rightarrow N0	N0 \rightarrow N3	N3 \rightarrow N0	N1 \rightarrow N2	N2 \rightarrow N1	N1 \rightarrow N3	N3 \rightarrow N1	N2 \rightarrow N3	N3 \rightarrow N2
WL subtree	50.1	59.9	50.9	51.0	51.8	54.5	56.7	57.0	52.5	57.6	54.4	46.9
GCN	53.7 \pm 2.1	68.2 \pm 1.9	50.6 \pm 1.9	45.8 \pm 1.7	35.5 \pm 2.4	28.2 \pm 2.2	55.9 \pm 1.7	56.8 \pm 1.9	55.7 \pm 1.5	53.2 \pm 2.1	60.4 \pm 1.8	54.8 \pm 0.9
GIN	51.4 \pm 1.7	47.5 \pm 2.1	50.4 \pm 1.6	32.7 \pm 1.6	47.0 \pm 2.1	29.4 \pm 2.3	52.4 \pm 1.9	55.7 \pm 2.0	64.3 \pm 1.8	51.1 \pm 1.2	60.3 \pm 1.3	53.5 \pm 1.6
GMT	53.0 \pm 1.9	58.3 \pm 1.7	49.0 \pm 1.9	34.3 \pm 1.6	39.7 \pm 1.5	27.5 \pm 2.4	55.8 \pm 1.6	60.4 \pm 2.1	51.3 \pm 1.0	51.5 \pm 1.6	60.0 \pm 2.6	54.5 \pm 1.4
CIN	54.5 \pm 2.1	36.8 \pm 1.9	53.0 \pm 1.3	32.7 \pm 2.1	44.9 \pm 1.4	27.4 \pm 1.1	58.4 \pm 1.6	54.2 \pm 2.3	63.9 \pm 1.6	51.2 \pm 1.4	64.7 \pm 1.1	53.7 \pm 2.1
PathNN	56.4 \pm 1.4	65.5 \pm 1.4	54.6 \pm 1.5	60.9 \pm 1.8	46.7 \pm 2.1	35.5 \pm 1.9	57.6 \pm 1.8	60.6 \pm 1.2	61.9 \pm 1.8	53.9 \pm 2.0	65.1 \pm 1.8	52.5 \pm 1.5
SFDA_LLN	57.9 \pm 1.9	72.7 \pm 2.1	54.3 \pm 1.9	71.6 \pm 2.0	65.7 \pm 1.5	72.6 \pm 2.0	58.0 \pm 1.8	61.1 \pm 2.0	68.2 \pm 1.7	58.9 \pm 2.3	64.2 \pm 1.5	58.7 \pm 1.8
SF(DA) ²	58.4 \pm 1.4	73.3 \pm 1.5	56.3 \pm 2.0	72.7 \pm 1.8	65.0 \pm 1.7	73.0 \pm 2.1	59.7 \pm 1.5	61.3 \pm 2.0	67.7 \pm 1.5	59.8 \pm 1.9	66.5 \pm 2.0	61.3 \pm 2.1
NVC_LLN	59.7 \pm 2.3	74.5 \pm 2.2	56.0 \pm 2.0	72.4 \pm 1.7	66.7 \pm 2.5	72.4 \pm 2.0	61.9 \pm 1.5	63.0 \pm 1.9	68.9 \pm 1.6	61.0 \pm 2.0	68.2 \pm 1.8	62.2 \pm 1.9
Ucon_SFDA	58.7 \pm 1.1	73.6 \pm 0.5	57.4 \pm 2.2	72.7 \pm 2.0	64.5 \pm 1.3	73.4 \pm 1.4	63.3 \pm 2.7	59.5 \pm 3.0	68.7 \pm 1.9	62.2 \pm 2.4	68.4 \pm 1.1	61.2 \pm 1.0
SOGA	60.9 \pm 1.3	74.6 \pm 2.0	54.9 \pm 1.8	72.6 \pm 2.2	68.0 \pm 1.4	72.6 \pm 1.3	64.2 \pm 1.6	65.0 \pm 1.7	68.2 \pm 1.0	61.8 \pm 0.8	67.9 \pm 2.0	63.8 \pm 1.7
GraphCTA	61.3 \pm 1.2	75.2 \pm 1.6	56.8 \pm 2.0	75.0 \pm 1.6	67.5 \pm 1.2	75.4\pm1.6	63.6 \pm 2.1	61.0 \pm 1.5	68.3 \pm 0.9	62.3 \pm 1.0	68.3 \pm 1.6	63.2 \pm 1.5
GALA	62.1 \pm 1.3	76.2 \pm 1.1	57.1 \pm 2.1	74.8 \pm 1.8	67.9 \pm 1.3	73.9 \pm 2.0	64.1 \pm 1.6	63.3 \pm 1.2	69.7 \pm 2.0	63.0 \pm 1.7	69.7 \pm 2.3	64.2 \pm 0.8
GraphATA	62.0 \pm 0.8	75.1 \pm 3.1	59.1 \pm 0.9	73.9 \pm 1.3	68.9\pm2.0	74.0 \pm 2.5	62.8 \pm 0.8	64.0 \pm 0.4	67.0 \pm 2.2	63.5 \pm 2.1	68.2 \pm 1.9	66.4 \pm 1.3
S ² PLR	68.4\pm2.0	83.7\pm1.4	62.3\pm2.3	75.3\pm1.6	66.4 \pm 2.3	73.5 \pm 3.1	70.8\pm0.4	74.2\pm0.6	71.1\pm0.6	63.8\pm1.5	76.4\pm2.3	70.5\pm1.8

TABLE XXV: ROC-AUC results (in %) on the ogbg-molhiv dataset under edge density domain shift (source \rightarrow target). H0, H1, H2, and H3 denote the sub-datasets partitioned with edge density. **Bold** results indicate the best performance.

Methods	H0 \rightarrow H1	H1 \rightarrow H0	H0 \rightarrow H2	H2 \rightarrow H0	H0 \rightarrow H3	H3 \rightarrow H0	H1 \rightarrow H2	H2 \rightarrow H1	H1 \rightarrow H3	H3 \rightarrow H1	H2 \rightarrow H3	H3 \rightarrow H2
WL	45.4	54.9	44.9	46.7	54.4	52.2	53.7	46.0	56.1	45.3	51.1	50.8
GCN	57.5 \pm 1.8	58.0 \pm 1.5	56.1 \pm 2.1	54.3 \pm 1.2	54.1 \pm 1.4	50.9 \pm 1.4	61.2 \pm 1.6	54.8 \pm 1.9	54.9 \pm 2.1	56.6 \pm 1.4	65.4 \pm 2.0	58.1 \pm 1.6
GIN	58.1 \pm 1.1	55.3 \pm 1.2	49.7 \pm 1.5	55.2 \pm 2.2	55.5 \pm 1.9	50.5 \pm 2.0	55.1 \pm 1.3	58.8 \pm 1.2	56.6 \pm 1.6	50.0 \pm 1.1	56.8 \pm 1.8	56.2 \pm 1.6
GMT	50.7 \pm 1.0	57.5 \pm 1.7	51.1 \pm 2.1	58.8 \pm 1.5	59.8 \pm 1.4	52.0 \pm 1.4	57.0 \pm 1.8	55.4 \pm 1.0	54.0 \pm 1.7	54.9 \pm 1.0	58.1 \pm 1.3	52.0 \pm 1.3
CIN	51.8 \pm 1.4	54.1 \pm 1.7	53.6 \pm 1.4	57.3 \pm 1.6	56.9 \pm 1.7	53.9 \pm 1.3	54.5 \pm 1.7	63.6 \pm 2.1	54.2 \pm 1.2	56.9 \pm 1.8	57.6 \pm 1.3	58.7 \pm 1.2
PathNN	57.3 \pm 1.1	57.8 \pm 2.0	54.8 \pm 1.9	53.2 \pm 1.1	49.8 \pm 1.6	57.9 \pm 1.9	60.2 \pm 1.6	63.7 \pm 1.5	42.2 \pm 1.8	58.1 \pm 2.2	49.6 \pm 1.5	60.5 \pm 1.3
SFDA_LLN	63.5 \pm 1.2	63.1 \pm 1.9	62.7 \pm 1.7	61.9 \pm 1.2	62.8 \pm 0.6	60.8 \pm 1.2	63.6 \pm 1.6	64.2 \pm 1.6	67.2 \pm 1.8	61.9 \pm 1.4	67.1 \pm 1.4	61.7 \pm 1.7
SF(DA) ²	63.6 \pm 0.3	63.7 \pm 1.2	63.6 \pm 0.6	61.8 \pm 0.2	64.7 \pm 0.7	58.6 \pm 3.2	63.9 \pm 0.5	64.4 \pm 0.5	64.6 \pm 0.4	61.5 \pm 1.6	65.1 \pm 0.9	62.7 \pm 1.8
NVC_LLN	58.8 \pm 2.2	60.7 \pm 0.5	59.6 \pm 1.1	60.9 \pm 0.7	62.8 \pm 2.7	60.6 \pm 0.6	60.2 \pm 1.8	60.5 \pm 1.9	64.9 \pm 1.6	61.8 \pm 0.4	62.6 \pm 2.0	61.1 \pm 0.7
Ucon_SFDA	60.8 \pm 0.7	62.3 \pm 2.1	61.0 \pm 1.6	62.5 \pm 3.1	65.3 \pm 1.9	60.7 \pm 1.5	62.1 \pm 2.2	62.7 \pm 1.0	68.3 \pm 1.5	62.5 \pm 1.3	63.1 \pm 0.8	61.5 \pm 1.2
SOGA	62.6 \pm 2.2	64.1 \pm 2.2	61.5 \pm 1.8	60.9 \pm 1.9	64.3 \pm 2.4	61.4 \pm 1.3	62.5 \pm 2.7	66.3 \pm 1.5	68.4 \pm 1.5	63.0 \pm 1.6	68.9 \pm 1.0	64.4 \pm 2.3
GraphCTA	61.5 \pm 1.5	63.9 \pm 1.1	61.9 \pm 1.9	60.8 \pm 1.3	63.4 \pm 1.7	61.0 \pm 2.1	63.5 \pm 1.4	66.9 \pm 1.4	67.9 \pm 1.2	64.4 \pm 1.8	69.6 \pm 1.2	66.0 \pm 1.3
GALA	63.8 \pm 1.5	64.6 \pm 1.3	62.7\pm1.6	61.1 \pm 1.4	64.0 \pm 1.3	61.3 \pm 1.9	64.2 \pm 1.5	66.7 \pm 1.4	68.4 \pm 1.3	64.6 \pm 1.5	70.9 \pm 1.5	65.1 \pm 1.5
GraphATA	63.3 \pm 1.1	66.3 \pm 0.3	62.6 \pm 0.3	60.9 \pm 1.2	63.2 \pm 2.4	64.2 \pm 0.7	62.3 \pm 0.8	64.2 \pm 1.7	68.0 \pm 0.6	70.2 \pm 0.4	69.7 \pm 1.2	70.3 \pm 0.5
S ² PLR	64.1\pm1.4	71.7\pm2.4	61.7 \pm 2.1	69.0\pm2.7	66.2\pm1.5	65.0\pm1.0	67.2\pm1.0	77.1\pm0.2	69.4\pm2.7	72.2\pm2.6	71.1\pm3.0	75.7\pm1.8